Disruption of the plastid-hosted iron-sulfur cluster biogenesis pathway in *Toxoplasma gondii* has pleiotropic effects irreversibly impacting parasite viability

Eléa A. Renaud[1‡], Sarah Pamukcu[1‡], Aude Cerutti[1], Laurence Berry[1], Catherine Lemaire-Vieille[2], Yoshiki Yamaryo-Botté[2], Cyrille Y. Botté[2], and Sébastien Besteiro[1*]

[1] LPHI, Univ Montpellier, CNRS, UMR5235, Montpellier, France

[2] ApicoLipid Team, Centre National de la Recherche Scientifique, Institute for Advanced Biosciences, Institut National de la Santé et de la Recherche Médicale, UMR5309, U1209, Université Grenoble Alpes, Grenoble, France

[‡] These authors contributed equally to this work; author order was determined randomly

[*] For correspondence: Sébastien Besteiro, sebastien.besteiro@inserm.fr

Running title: Importance of the Toxoplasma SUF iron-sulfur cluster pathway

Keywords: Toxoplasma gondii, iron metabolism, iron-sulfur protein, parasite metabolism, apicoplast, lipid

Abstract

Like many other apicomplexan parasites, *Toxoplasma gondii* contains a plastid harbouring key metabolic pathways, including the SUF pathway that is involved in the biosynthesis of iron-sulfur clusters. These cofactors are key for a variety of proteins involved in important metabolic reactions, potentially including plastidic pathways for the synthesis of isoprenoid and fatty acids. It was shown previously that impairing the NFS2 cysteine desulfurase, involved in the first step of the SUF pathway, leads to an irreversible killing of intracellular parasites. However, the metabolic impact of disrupting the pathway remained unexplored. We have generated another mutant of the pathway, deficient for the SUFC ATPase, and we have investigated in details the phenotypic consequences of TgNFS2 and TgSUFC depletion on parasite homeostasis. Our analysis confirms that Toxoplasma SUF mutants are severely and irreversibly impacted in growth: cell division and membrane homeostasis are particularly affected. Lipidomic analysis suggests a defect in apicoplast-generated fatty acids, along with a simultaneous increase in scavenging of host-derived lipids. However, addition of exogenous lipids did not allow full restauration of growth, suggesting other more important cellular functions were impacted in addition to fatty acid synthesis. For instance, we have shown that the SUF pathway is also key for generating isoprenoid-derived precursors necessary for the proper targeting of GPI-anchored proteins as well as for the parasite gliding motility. Thus, plastid-generated iron-sulfur clusters support the functions of proteins involved in several vital downstream cellular pathways, which implies the SUF machinery may be explored for discovering new potential anti-Toxoplasma targets.

40

41

42 *Introduction*

43 Apicomplexan parasites are some of the most prevalent and morbidity-causing pathogens
44 worldwide. Noticeably, they comprise *Plasmodium* species that can naturally infect humans and
45 cause the deadly malaria in tropical and subtropical areas of the world (1). Although less lethal,
46 another apicomplexan parasite called *Toxoplasma gondii* can cause serious illness in animals,
47 including humans, and has a widespread host range and geographical distribution (2). These protists
48 are obligate intracellular parasites that rely to a large extent on their host cells for nutrient
49 acquisition and for protection from the immune system. Through their evolutionary history,
50 *Plasmodium* and *Toxoplasma* have inherited a plastid from a secondary endosymbiosis event
51 involving the engulfment of a red alga whose photosynthetic capability previously originated from
52 the acquisition of a cyanobacterium (3). Although the ability to perform photosynthesis has been lost
53 during evolution when the ancestors of Apicomplexa became parasitic (4), the plastid has retained
54 critical metabolic functions. For instance it hosts pathways for the synthesis of heme (together with
55 the mitochondrion), fatty acids (FASII), isoprenoid precursors (through the so-called non-mevalonate
56 pathway), and iron-sulfur (Fe-S) clusters (5, 6). Because of its origin and its metabolic importance, the
57 apicoplast is particularly attractive to look for potential drug targets (7).

58 As some of the earliest catalytic cofactors on earth (8), Fe-S clusters are found in all kingdoms of life,
59 associated with proteins involved in a number of key cellular functions like the synthesis of
60 metabolites, the replication and repair of DNA, the biogenesis of ribosomes and the modification of
61 tRNAs (9). The biosynthesis of Fe-S clusters necessitates a complex machinery for assembling ferrous
62 (Fe^{2+}) or ferric (Fe^{3+}) iron and sulfide (S^{2-}) ions, and delivering the resulting Fe-S cluster to target
63 client proteins (10). In eukaryotes Fe-S proteins are present in various subcellular compartments like
64 the cytosol and the nucleus, but also organelles of endosymbiotic origin like mitochondria or plastids,
65 and thus require compartment-specific biogenesis systems. The three main eukaryotic Fe-S synthesis
66 pathways comprise the ISC (iron-sulfur cluster) machinery, hosted by the mitochondrion, the
67 cytosolic Fe-S protein assembly (CIA) machinery, important not only for the generation of cytosolic,
68 but also of nuclear Fe-S proteins, and the SUF (sulfur formation) pathway that is found in plastids (9).

69 Like in plants and algae, apicoplast-containing apicomplexan parasites seem to express the
70 machinery corresponding to the three eukaryotic pathways. For instance, in *T. gondii* recent
71 investigations have shown that the CIA, ISC and SUF pathways are all essential for parasite fitness
72 (11, 12). From a biochemical point of view, mitochondrial and plastidic Fe-S cluster biosynthesis
73 pathways follow a similar general pattern: cysteine desulfurases produce sulfur from L-cysteine, then
74 scaffold proteins provide a molecular platform allowing assembly of iron and sulfur into a cluster,
75 and finally carrier proteins deliver the cluster to target apoproteins. Importantly, targeting the *T.*
76 *gondii* mitochondrial ISC pathway through disruption of scaffold protein ISU1 was shown to lead to a
77 reversible growth arrest and to trigger differentiation into a stress-resistant form; while on the other
78 hand, targeting the plastidic SUF pathway by inactivating NFS2 function led to an irreversible lethal
79 phenotype (12). Like for many apicoplast-hosted pathways, enzymes belonging to the SUF machinery
80 are essentially absent from the mammalian host and as such they may be seen as good potential
81 drug targets. This has sparked considerable interest for the SUF pathway in *Plasmodium*, which has
82 been shown to be important for the viability of several developmental stages of the parasite (13–17).

83 To better understand the contribution of the SUF pathway to *T. gondii* viability, we have generated a
84 conditional mutant for the scaffold protein TgSUFC and conducted a thorough phenotypic

85 characterization of this mutant, together with the TgNFS2 mutant we have previously generated (12).
86 Our results confirm that inactivating the plastid-hosted SUF pathway in *T. gondii* leads to irreversible
87 and marked effects on membrane homeostasis, impacting the division process and parasite viability.
88 We show that these effects are likely due to impairment in the function of several key plastidic Fe-S
89 proteins, which have pleiotropic downstream metabolic consequences for the parasite.

90

91 *Results*

92 **A Toxoplasma SUFC homolog in the apicoplast**

93 Searching for homologs of the plant SUF system in the ToxoDB.org database, we have previously
94 shown an overall good conservation for the plastidic Fe-S cluster synthesis pathway (12). Among the
95 candidates for members of the SUF machinery, we have identified a potential *T. gondii* homolog of
96 SUFC, member of a Fe-S cluster scaffold complex comprising SUFC, SUFB and SUFD (Fig. 1A). This
97 complex is also present in prokaryotes, where it was first characterized (18): it was shown that
98 bacterial SufC is an ATP-binding cassette (ABC)-like ATPase component essential for proper Fe-S
99 cluster assembly (19). Alignment of the amino acid sequences of the *T. gondii* SUFC candidate (entry
100 TGGT1_225800 in the ToxoDB.org database (20)) and its *Escherichia coli* counterpart showed a good
101 overall conservation (56% of identity), particularly in the motifs that are characteristic of ABC
102 ATPAses (Fig. 1B). The *T. gondii* protein presents a N-terminal extension when compared with *E. coli*
103 SufC, which may contain a transit peptide for targeting to the apicoplast. Accordingly, it was
104 predicted with high probability to be a plastid-localized protein by the Deeploc 1.0
105 (http://www.cbs.dtu.dk/services/DeepLoc-1.0/) algorithm, although the exact position of the N-
106 terminal transit peptide sequence could not be defined. Data from global mapping of *T. gondii*
107 proteins subcellular location by hyperLOPIT spatial proteomics (21) also suggested an apicoplast
108 localization for TGGT1_225800. To assess whether this protein is a real functional homolog, we first
109 performed complementation assays of an *E. coli* SufC mutant, for which growth is slowed, especially
110 when limiting iron availability with a specific chelator (22). We could show that expressing the
111 predicted functional domain of TGGT1_225800 restored bacterial growth (Fig. 1C), even in the
112 presence of the iron chelator, confirming this protein (hereafter named TgSUFC) is functional.

113 In order to detect TgSUFC expression and assess its sub-cellular localization in the tachyzoite stage
114 (the fast-replicating stage associated with acute toxoplasmosis (2)), we epitope-tagged the native
115 protein. This was performed by inserting a sequence coding for a C-terminal triple hemagglutinin
116 (HA) epitope tag at the endogenous *TgSUFC* locus by homologous recombination (Figure S1). It was
117 achieved in the TATi ΔKu80 cell line, favoring homologous recombination and allowing
118 transactivation of a Tet operator-modified promoter that we subsequently used for generating a
119 conditional mutant in this background (23–25). Immunoblot analysis with an anti-HA antibody
120 revealed two products, likely corresponding to the immature and mature forms (resulting from the
121 cleavage of the transit peptide upon import into the organelle) of TgSUFC (Fig. 2A).
122 Immunofluorescence assay (IFA) with the anti-HA antibody and co-staining with an apicoplast marker
123 confirmed that TgSUFC localizes to this organelle in *T. gondii* tachyzoites (Fig. 2B).

124

125 **Depletion of TgSUFC blocks parasite growth**

126 Next, we generated a conditional TgSUFC mutant cell line in the TgSUFC-HA-expressing TATi ΔKu80
127 background. Replacement of the endogenous promoter by an inducible-Tet07SAG4 promoter was

128 achieved through a single homologous recombination at the locus of interest, yielding the cKD
129 TgSUFC-HA cell line (Fig. S2). In this cell line, the addition of anhydrotetracycline (ATc) can repress
130 transcription through a Tet-Off system (26). Initial phenotypic characterization was performed on
131 two independent clones, which were found to behave similarly and thus only one was analysed
132 further. It should be noted that the promoter replacement resulted in a slightly higher expression of
133 TgSUFC, but did not change the maturation profile of the protein (Fig. 2A). Down-regulation of
134 TgSUFC was assessed by growing the parasites in the presence of ATc. Immunoblot and IFA analyses
135 showed a decrease of TgSUFC to almost undetectable levels after as early as one day of ATc
136 treatment (Fig. 2A and B). We also generated a complemented cell line constitutively expressing an
137 additional TY-tagged (27) copy of TgSUFC from the *uracil phosphoribosyltransferase* (*UPRT*) locus,
138 driven by a *tubulin* promoter (Fig. S3). This cell line, named cKD TgSUFC-HA comp, was found by
139 immunoblot (Fig. 2C) and IFA (Fig. 2D), to be stably expressing TgSUFC while the HA-tagged copy was
140 down-regulated in the presence of ATc.

141 We first evaluated the consequences of TgSUFC depletion on parasite fitness *in vitro* by performing a
142 plaque assay, which determines the capacity of the mutant and complemented parasites to produce
143 lysis plaques on a host cells monolayer in absence or continuous presence of ATc for 7 days (Fig. 3).
144 Depletion of TgSUFC prevented plaque formation, which was restored in the complemented cell lines
145 (Fig. 3A and B). Our previous analysis of another SUF pathway mutant (TgNFS2, (12)) suggested that
146 the impact on the pathway leads to irreversible death of the parasites, so we sought to verify this by
147 removing the ATc after 7 days of incubation and monitoring plaque formation. We confirmed that
148 depleting TgSUFC was irreversibly impacting parasite viability, as ATc removal did not lead to the
149 appearance of plaques (Fig. 3C). We next assessed whether this defect in the lytic cycle is due to a
150 replication problem. Mutant and control cell lines were preincubated in absence or presence of ATc
151 for 48 hours and released mechanically, before infecting new host cells and were then grown for an
152 additional 24 hours in ATc prior to parasite counting. We noted that the incubation with ATc led to
153 an accumulation of vacuoles with fewer TgSUFC mutant parasites, but that it was not the case in the
154 complemented cell lines (Fig. 3D). Overall, our data show that depleting TgSUFC leads to an
155 irreversible impact on parasite growth, as previously described for other SUF mutant TgNFS2 (12).

156

157 **SUF pathway mutants display important membrane defects during cell division**

158 *T. gondii* tachyzoites divide by a process called endodyogeny, whereby two daughter cells will
159 assemble inside a mother cell (28). Among the structures which are essential as a scaffold for
160 daughter cell formation is the inner membrane complex (IMC), a system of flattened vesicles
161 underlying the plasma membrane and is supported by a cytoskeletal network. The IMC also supports
162 anchorage for the glideosome, the protein complex powering parasite motility (29). As for several
163 other cellular structures, there is a combination of *de novo* assembly and recycling of maternal
164 material during IMC formation in daughter cells (30). To get more precise insights into the impact of
165 the impairment of the SUF pathway on parasite division, we incubated the TgNFS2 and TgSUFC
166 mutant parasites with ATc for up to 2 days and stained them for IMC protein IMC3 to detect growing
167 daughter cells (Fig. 4A). IMC3 is an early marker of daughter cell budding (31), which is usually
168 synchronized within the same vacuole. However, after two days of ATc treatment an increasing
169 portion of the vacuoles showed a lack of synchronicity for daughter cell budding for both mutant cell
170 lines, although the effect was more pronounced for the TgSUFC mutant (Fig. 4A and B).

171 Then, we used electron microscopy to get a subcellular view of the consequences of TgNFS2 and
172 TgSUFC depletion on the cell division process. Strikingly, in parasites grown in the continuous

173 presence of ATc for three days, we observed cytokinesis completion defects. As budding daughter
174 cells emerge, they normally incorporate plasma membrane material that is partly recycled from the
175 mother, leaving only a basal residual body. Here, in both TgNFS2 and TgSUFC mutant cell lines
176 daughter cells remained tethered through patches of plasma membrane (Fig. 4C). However, most
177 membrane-bound subcellular compartments seemed to have an otherwise normal morphology.
178 Hence, this highlighted an early and important defect in plasma membrane synthesis and/or
179 segregation during daughter cell budding. We previously observed major cell division defects after
180 long term (five days or more) continuous incubation of cKD TgNFS2-HA parasites with ATc (12). When
181 assessing the cKD TgSUFC-HA parasites in the same conditions, co-staining with apicoplast and IMC
182 markers revealed similar defects, including organelle segregation problems and an abnormal
183 membranous structures (Fig. 4D).

184

185 **Depletion of TgSUFC has an impact on the apicoplast**

186 Computational prediction of the Fe-S proteome combined with hyperLOPIT localization data suggests
187 there is a limited number of apicoplast proteins potentially containing Fe-S clusters (12). However,
188 these candidates are supposedly very important for the parasite. They include: IspG and IspH, two
189 oxidoreductases involved in isoprenoid synthesis (32); LipA, a lipoyl synthase important for the
190 function of the pyruvate dehydrogenase (PDH) complex (33); MiaB, which is likely a tRNA
191 modification enzyme (34); as well as of course proteins that are directly involved in Fe-S synthesis,
192 and the plastidic ferredoxin (Fd) that is an important electron donor that regulates several
193 apicoplast-localized pathways (35–37). Dataset from a CRISPR-based genome-wide screen suggests
194 that most of these candidates are important for fitness *in vitro* (38).

195 We first assessed whether depletion of TgSUFC led to a partial apicoplast loss, as was previously
196 shown for TgNFS2 (12). Although slowed down in growth, some parasites eventually egressed during
197 the course of the experiments and were used to reinvade host cells, and were kept for a total of 5
198 days in the presence of ATc (Fig. 5A). This is reminiscent to the so-called "delayed death" effect,
199 observed when inhibiting apicoplast metabolism, that often results in slow-kill kinetics (39).
200 Quantification of the apicoplast marker TgCPN60 showed a progressive loss of this protein (Fig. 5A
201 and B). As this could reflect a specific impact on this protein marker rather than a general loss of the
202 organelle, we also stained the parasites with fluorescent streptavidin (mainly detects the biotinylated
203 apicoplast protein acetyl-CoA carboxylase (40)), confirming a similar loss of signal after 5 days of
204 incubation with ATc (Fig. S4). This suggests TgSUFC depletion leads to a progressive but late loss of
205 the apicoplast. Of note, this effect on the organelle is less marked than when TgNFS2 is depleted
206 (12).

207 One of the apicoplast-localized Fe-S proteins whose activity can be assessed is LipA, which is
208 responsible for the lipoylation of a single apicoplast target protein, the E2 subunit of the PDH (41).
209 We performed an immunoblot analysis with an anti-lipoic acid on protein extracts from cKD TgSUFC-
210 HA parasites kept in the presence of ATc for up to 4 days (Fig. 5 C and D). We noticed a progressive
211 decrease in lipoylated PDH-E2 to almost no signal after 3 days of ATc incubation. Using an antibody
212 that we specifically raised against the E2 subunit of the PDH, we verified this was not due to a
213 decrease in global levels of this particular protein. Overall, this is comparable to what we previously
214 described upon depletion of TgNFS2 (12). Thus, disrupting the SUF pathway has direct consequences
215 on Fe-S proteins-dependent metabolic pathways hosted by the apicoplast, and prolonged depletion
216 of SUF proteins can even lead to partial loss of the organelle.

217

218 **Impact of SUF pathway disruption on fatty acid metabolism**

219 The PDH complex generates acetyl-CoA, which is the first step of the FASII system in the apicoplast.
220 This pathway generates fatty acid (FA) precursors that are subsequently elongated in the
221 endoplasmic reticulum (ER) (42), to generate for instance essential membrane building blocks. We
222 first wanted to evaluate the impact of the perturbation of the SUF pathway on parasite lipids. Total
223 lipids from the TgNFS2 and TgSUFC mutant cell lines were determined by gas chromatography-mass
224 spectrometry (GC-MS). For the NFS2 mutant we noted small but significant decrease in abundance of
225 shorter FAs (C12-C17), suggesting de novo FA synthesis is affected (Fig. 6A), however this was not as
226 clear for the SUFC mutant (Fig. 6B).

227 While FASII was shown previously to be important for tachyzoite fitness (41), recent investigations
228 have shown that tachyzoites are able to scavenge FA precursors from their host cells and at least
229 partly compensate for lack of de novo synthesis (43, 44). To investigate whether the SUFC mutant
230 may also be affected in apicoplast FA synthesis but may have developed a compensatory mechanism,
231 we thus sought to assess the impact of TgSUFC depletion on *de novo*-synthesized versus scavenged
232 lipids by stable isotope precursor labeling with ^{13}C glucose combined with mass spectrometry-based
233 lipidomic analyses (43, 45). These analyses highlighted an increase in scavenging from the host cells is
234 happening in absence of TgSUFC, as shown for the C16:0 FA (Fig. 6C). This reflects most likely a
235 mechanism for compensating the lack of *de novo*-made FAs by increasing scavenging host-derived
236 FAs.

237 The ability of tachyzoites to survive lack of de novo lipid synthesis is highly dependent on the
238 availability of exogenous lipid precursors. Others have shown that FASII mutants could be rescued by
239 the addition of palmitic (C16:0) or myristic (C14:0) acid for instance (42, 44, 46). We thus tried to
240 compensate the impact of TgNFS2 and TgSUFC depletion on the parasite lipid homeostasis by
241 supplementing the growth medium with these FAs and performing plaque assays. Palmitic acid
242 supplementation partially restored growth of the TgNFS2 mutant (Fig. 7A and B), while with myristic
243 acid only after long term incubation (up to two weeks) these mutant parasites started growing back
244 (Fig. 7C and D). In contrast, depletion of TgSUFC was not efficiently compensated by exogenous fatty
245 supplementation (Fig. 7). As our lipidomic analysis has shown that depletion of TgNFS2 affects de
246 novo lipid production (Fig. 6A), so it makes sense that providing exogenous lipids can improve fitness
247 of the mutant parasites. On the other hand, TgSUFC mutant parasites are likely able to scavenge
248 lipids from the host as a compensation for an altered de novo synthesis (Fig. 6C), and medium
249 supplementation with more exogenous lipids does not seem to further improve their fitness.

250 This highlights differences between the two SUF pathway mutants with regards to adaptation to the
251 perturbation of lipid homeostasis, which may be explained by different kinetics in depletion of the
252 respective proteins, or a different impact on global apicoplast function. In any case, our data
253 confirms apicoplast-based lipid production is affected in SUF pathway mutants, and while these
254 parasites establish compensatory mechanisms by scavenging exogenous lipid precursors, they do not
255 allow them recovering to full fitness. This suggests that perturbation of apicoplast FA synthesis is not
256 the only, and perhaps not even the primary, effect of SUF pathway disruption impacting growth.

257

258 **SUF pathway disruption also has an impact on isoprenoid-dependent pathways**

259 The other main apicoplast-localized biosynthetic pathway potentially affected by disruption of the
260 SUF machinery is isoprenoid synthesis, through the two Fe-S-containing proteins IspG and IspH that
261 are needed for the synthesis of the five carbon precursor isopentenyl pyrophosphate (IPP) and its

262 isomer dimethylallyl pyrophosphate (DMAPP) (32). Synthesis of these isoprenoid building blocks is
263 the only essential metabolic function of the apicoplast in the asexual intraerythrocytic stages of
264 *Plasmodium*, where the loss of the organelle can be simply compensated by supplementation with
265 exogenous IPP (47). *Plasmodium* SUF mutants survive when cultured in the presence of IPP,
266 confirming the essential role of the Fe-S synthesizing pathway in this parasite is likely for isoprenoid
267 synthesis (13). Isoprenoid synthesis is also vital for *T. gondii* tachyzoites (48), however IPP
268 supplementation to the culture medium is not possible because, unlike for *Plasmodium,* the highly
269 charged IPP does not efficiently reach the parasite cytoplasm. Tachyzoites can nevertheless scavenge
270 some isoprenoids precursors from their host cells (49). Apicoplast-derived isoprenoid precursors are
271 mostly known for their involvement in important posttranslational protein modifications like
272 prenylation, glycosylphosphatidylinositol (GPI) anchoring, as well glycosylation, in addition to the
273 synthesis of quinones and several antioxidant molecules (32).

274 In *Plasmodium* it is believed that prenylated proteins that regulate vesicle trafficking are key in the
275 delayed death phenotype caused by apicoplast loss (50). As geranylgeraniol (GGOH), an isoprenoid
276 precursor for protein farnesylation/prenylation, was successfully used to at least partially
277 complement deficiencies in apicoplast isoprenoid production (49, 51), we tried to supplement the
278 culture medium with GGOH and perform plaque assays with the SUF mutants we generated.
279 However, we did not detect any restoration of growth (Fig. S5A). In contrast to *Plasmodium* (52, 53),
280 the prenylome of *T. gondii* is still largely uncharacterized, but using an anti-farnesyl antibody, we did
281 not detect obvious alterations in the general profile of prenylated proteins upon depletion of TgNFS2
282 or TgSUFC (Fig. S5B). Although apicoplast-generated IPP and DMAPP are also necessary for
283 synthesizing the farnesyl diphosphate used for protein prenylation in *T. gondii* tachyzoites, it is thus
284 possible that these parasites can initially scavenge host-derived isoprenoids to compensate for a
285 deficient *de novo* production (49). In any case, altogether our results suggest that defects in protein
286 farnesylation/prenylation may not be one of the primary consequences of SUF pathway disruption in
287 *T. gondii*.

288 We next sought to investigate the potential impact of TgNFS2 or TgSUFC depletion on GPI anchoring.
289 The SAG-related sequence (SRS) family comprising proteins related to SAG1, the first characterized *T.*
290 *gondii* surface antigen, is arguably the best characterized family of GPI-anchored proteins in the
291 parasite (54). We pre-incubated mutant parasites for three days with ATc, and allowed them to
292 invade and grow into host cells for an extra day in the presence of ATc before using specific
293 antibodies to detect GPI-anchored SAG1 and SAG3. We could see obvious signs of mislocalization for
294 these two proteins that, instead of keeping a homogenous peripheral distribution, they were often
295 seen accumulated at the apex or base of the parasites, or found within the parasitophorous vacuole
296 space (Fig. 8A and B). Interestingly, while the SAG1 protein appears to be distributed differently by
297 IFA, our previous immunoblot analyses suggest there is no drastic change in the total amount of
298 protein upon TgNFS2 or TgSUFC depletion ((12) and Fig. 2A). It was previously shown that the
299 deletion of SAG1's GPI anchor leads to a constitutive secretion of this protein to the parasitophorous
300 vacuole space (55). It should be noted that, in contrast to the distribution of GPI-anchored SAG
301 proteins, in these experimental conditions the overall structure of the IMC appeared unaffected (Fig.
302 8A and B). Hence, our data suggest that disruption of the SUF pathway perturbs GPI anchor
303 formation.

304 Another important posttranslational modification depending on isoprenoid-containing dolichol is
305 glysosylation. Several key proteins of the glideosome complex are supposedly glycosylated, and as a
306 consequence glycosylation inhibition has been reported to impact parasite motility (56, 57). We thus
307 performed gliding motility assays on the SUF mutants. Typically, this is done by monitoring the

308 shedding of SAG1, that leaves trails when tachyzoites glide on solid substrates. Perhaps as a
309 consequence of SUF pathway disruption on SAG1 targeting, trails they were clearly less abundant
310 upon depletion of TgNFS2 and TgSUFC (Fig. 8C and D). We could nevertheless detect and measure
311 trails, whose mean length provides an estimate of overall motility rates, and they were found to be
312 significantly smaller in absence of TgNFS2 or TgSUFC (Fig. 8E). These results suggest that protein
313 glycosylation is also affected upon disruption of the SUF pathway. Overall, our findings indicate that
314 the depletion of proteins of the SUF pathway leads to defects in the synthesis of isoprenoids
315 precursors with consequences on the post-translational modification and targeting of proteins of the
316 peripheral membrane system.

317

318 *Discussion*

319 Beside components of the SUF Fe-S cluster synthesis machinery, the apicoplast harbors only a small
320 number of putative Fe-S proteins (Fig. 9, (12)). Yet, they are all presumably important for parasite
321 fitness as suggested by their negative scores with a CRISPR-based genome-wide screen (Fig. 9, (38)).
322 However, not all are expected to be absolutely essential *in vitro*, tRNA modifying enzyme MiaB for
323 instance, has only a moderately low fitness score and has been shown recently in to be dispensable
324 for *Plasmodium* intraerythrocytic stages (37). Similarly, the LipA lipoyl synthase essential for the
325 function of the E2 subunit of the PDH complex, which is in turn crucial for generating the acetyl-CoA
326 necessary for de novo FA synthesis in the apicoplast, seems dispensable for *Plasmodium* blood stages
327 (37), for which the FASII system is not essential (58). However, given the potentially greater
328 importance of FASII in *T. gondii* tachyzoites (41), this is something we investigated further. We
329 demonstrated disruption of the SUF pathway impaired LipA function and PDH-E2 lipoylation (Fig. 5)
330 and, likely as a consequence of this and FASII perturbation, general production of myristic and
331 palmitic acid in the parasites (Fig. 6). However, the growth defect of SUF mutants could only be
332 partially complemented by FA supplementation for the TgNFS2 mutant, and not at all for the TgSUFC
333 mutant (Fig. 7), suggesting perturbation of FASII is not the primary cause of death for these mutants.
334 While it is undoubtedly a metabolic pathway that plays a central role for parasite fitness, the view on
335 the essentiality of FASII in *T. gondii* tachyzoites has recently evolved. There is now published
336 evidence that parasites can survive *in vitro* even when FASII enzymes are inactivated (44, 59) and
337 there is clearly flexibility in the adaptation to lipid sources (60). As tachyzoites can readily scavenge
338 and incorporate FAs from exogenous sources into their own range of lipids (43, 44, 61), in the end
339 the essentiality of the FASII pathway depends largely on the culture conditions.

340 The other main metabolic pathway that depends directly on Fe-S proteins in the apicoplast is for the
341 synthesis of isoprenoid precursors. When their isoprenoid production is inhibited, *T. gondii*
342 tachyzoites can scavenge some of these precursors from the host cell, leading to a delayed death
343 effect (49, 62), but that cannot fully compensate for a lack of de novo synthesis. Isoprenoids are a
344 large and diverse class of lipids whose cellular functions in Apicomplexa still remain to be extensively
345 characterised, but they include synthesis of vitamins and cofactors (ubiquinone), and are also
346 involved in important posttranslational modifications of proteins, like prenylation, GPI-anchoring and
347 glycosylation (Fig. 9, (32)). Ubiquinone is a central molecule in the mitochondrial electron transport
348 chain (ETC): its quinone head is the functional group for the transfer of electrons, whereas the
349 isoprenoid tail primarily serves for anchoring to the inner mitochondrial membrane. The
350 mitochondrial ETC is a validated drug target in Apicomplexa, for which complex III inhibitor
351 atovaquone has been used in therapeutic strategies (63). However, while *T. gondii* mitochondrial ETC
352 mutants are severely impaired in growth (64–67), it seems that genetic or pharmaceutical
353 inactivation (with atovaquone) is reversible ((12, 66)), and may lead to stage conversion and a

354 metabolic dormant state rather than complete death of the parasites. On the contrary, the viability
355 of the SUF mutants is irreversibly affected (Fig. 3C and (12)). So although the impact SUF protein
356 depletion on the isoprenoid pathway is likely to lead to a deficiency in ubiquinone synthesis, which in
357 turn would contribute to a decrease in parasite fitness, this is probably not the main reason for the
358 irreversible death of the parasites.

359 In *Plasmodium* blood stages, where isoprenoid synthesis is the only essential pathway hosted by the
360 apicoplast, disrupting the prenylation of Rab GTPAses, which are involved in vesicular trafficking,
361 contributes to delayed death (50). In *T. gondii*, interestingly, perturbation of Rab function can lead to
362 intracellular accumulation and patchy surface distribution of SAG1 proteins, and results in defects in
363 the delivery of new membrane required for completing daughter cell segregation at the end of
364 cytokinesis (68, 69). This bears some similarity with some phenotypes we have observed in the SUF
365 mutants, yet while we cannot completely exclude Rab prenylation is perturbed in the SUF mutants,
366 we did not identify any particular prenylation problem in the parasites, and we failed to complement
367 their growth defect with prenylation precursor GGOH (Fig. S5). We thus investigated other important
368 isoprenoid-dependent protein modifications. For instance, upon sugar addition dolichol can be used
369 for the formation of GPI anchors, or act as a donor for protein glycosylation. Our phenotypic analysis
370 revealed that the targeting of GPI-anchored surface proteins and the gliding motility of the parasites,
371 which relies on glycosylated proteins, were clearly affected upon disruption of the SUF pathway (Fig.
372 8). This confirms the importance of the apicoplast Fe-S cluster synthesis machinery for isoprenoid
373 metabolism. In *Plasmodium*, interfering with apicoplast-hosted isoprenoid production affects the
374 morphology of the organelle (70) but depletion of IspG and IspH does not lead to loss of the
375 apicoplast (37), while interfering with the SUF pathway does (13). We also observe a late impact on
376 the organelle (Fig. 5), that suggest the phenotypic consequences of SUF proteins in *T. gondii* are
377 indeed multifactorial and would extend beyond the simple disruption of the isoprenoid pathway.

378 At the cellular level, one of the most visible consequence of long term depletion of SUF proteins is
379 the membrane defects in the late stages of cytokinesis (Fig. 4). Interestingly, treatment of tachyzoites
380 with the FASII inhibitor triclosan or inactivating the FASII component acyl carrier protein was shown
381 to lead to severe problems in cytokinesis completion, with tethered daughter cells resembling the
382 phenotype we have described here (46). A similar phenotype was also observed in the mutant for
383 TgATS2, an apicoplast-located acyltransferase (43). This points to a central role for the apicoplast to
384 provide specific precursors for membrane biogenesis during cytokinesis, and to a SUF-dependent
385 FASII function is important for the homeostasis of the parasite plasma membrane. It should however
386 be noted that some isoprenoid-dependent cellular mediators may also contribute to plasma
387 membrane synthesis during cell division. For instance, disruption of Rab-controlled vesicular
388 trafficking, leads to very similar phenotypes of incomplete cytokinesis, with tachyzoites still fused
389 along their lateral surface (68, 69). Glycosylated IMC proteins associated with gliding motility are also
390 important for IMC formation and the cell division process (71). It is also possible that yet unidentified
391 GPI-anchored *T. gondii* proteins may be involved in plasma membrane formation or recycling: GPI
392 synthesis is essential for *T. gondii* survival (72), but the function of individual GPI-anchored proteins
393 remain largely overlooked. The detrimental effects of SUF depletion on plasma membrane
394 homeostasis may thus manifest through both FASII and isoprenoid perturbation. Moreover, as some
395 isoprenoid-dependent modifications are also linked to FA acid synthesis, like GPI anchors of *T. gondii*
396 surface proteins that also necessitate phospholipid moieties (73), a simultaneous impact on the two
397 pathways may enhance the phenotypic output.

398 One key apicoplast-located Fe-S protein is Fd, which has a central role in the function of Fe-S-
399 dependent apicoplast enzymes: it is potentially providing electrons to other apicoplast Fe-S enzymes

400 like MiaB, IspG, IspH and LipA. The role of Fd has recently been investigated in Apicomplexa. In
401 *Plasmodium* blood stage, the loss of parasite viability upon Fd depletion was likely mostly due to the
402 importance of Fd for the isoprenoid synthesis pathway (37), which is the only essential apicoplast-
403 located pathway in this developmental stage. Fd is equally essential for *T. gondii*, tachyzoite survival,
404 where it was shown to impact both FASII and isoprenoid synthesis (35), in a similar fashion to our
405 SUF mutants. Whether the vital importance of Fe-S cluster synthesis and associated apicoplast redox
406 metabolism is solely through its key role in isoprenoid synthesis is thus less clear in *T. gondii* than in
407 *Plasmodium*. As *T. gondii* tachyzoites grow in host cell types that can potentially provide them with
408 more resources, the ability to scavenge exogenous metabolites creates a complex situation whereby
409 metabolic pathways like FASII may be only essential in certain particular conditions. The nutrient-rich
410 in vitro culture systems may also mask some important contributions. In any case, because of their
411 upstream role in cellular functions important for parasite fitness, Fd and SUF mutants clearly have
412 pleiotropic effects. More importantly, we have confirmed here that disrupting the SUF machinery
413 leads to an irreversible death of the tachyzoites, which is not the case, for example, when the
414 mitochondrial Fe-S cluster machinery is inactivated (12). For all these reasons, and also because of its
415 absence from mammalian hosts of the parasite, the SUF pathway has a strong potential identifying
416 novel drug targets.

417

418 *Experimental procedures*

419 **Parasites and cells culture.** Tachyzoites of the TATi ΔKu80 *T. gondii* strain (25), as well as derived
420 transgenic parasites generated in this study, were maintained by serial passage in monolayers of
421 human foreskin fibroblast (HFF, American Type Culture Collection, CRL 1634) grown in Dulbecco's
422 modified Eagle medium (Gibco), supplemented with 5% decomplemented fetal bovine serum, 2-mM
423 L-glutamine and a cocktail of penicillin-streptomycin at 100 µg/ml.

424

425 **Bioinformatic analyses.** Sequence alignment was performed using the MUltiple Sequence
426 Comparison by Log-Expectation (MUSCLE) algorithm of the Geneious 6.1.8 software suite
427 (http://www.geneious.com). Transit peptide and localization prediction was done with the Deeploc
428 1.0 (http://www.cbs.dtu.dk/services/DeepLoc-1.0/) algorithm.

429

430 **Heterologous expression in *E. coli*.** Construct for designing the recombinant protein used for *E. coli*
431 complementation was defined by aligning the amino acid sequences of TgSUFC with its *E. coli*
432 counterparts. A 894 bp fragment corresponding to amino acids 220-518, was amplified by
433 polymerase chain reaction (PCR) from *T. gondii* cDNA using primers ML4200/ML4010 (sequences of
434 the primers used in this study are found in Table S1). The fragment was cloned into the pUC19
435 plasmid (Thermo Fisher Scientific) using the HindIII/BamHI restriction sites. The SufC *E. coli* mutant
436 from the Keio collection (obtained from the The *Coli* Genetic Stock Center at the University of Yale:
437 stain number JW1672-1), was transformed with the plasmid expressing the TgSUFC recombinant
438 protein and selected with ampicillin. For growth assays (22), overnight stationary phase cultures
439 were adjusted to the same starting OD_{600} of 0.6 in salt-supplemented M9 minimal media containing
440 0.4% glucose and varying amounts of the 2,2′-Bipyridyl iron chelator (Sigma-Aldrich). Growth was
441 monitored through OD_{600} measurement after 7, 14 and 24 hours at 37°C in a shaking incubator.

442

443 **Generation of the HA-tagged TgSUFC cell line.**

444 A CRISPR-based strategy was used. Using the pLIC-HA_3-CAT plasmid as a template, a PCR was
445 performed with the KOD DNA polymerase (Novagen) to amplify the tag and the resistance gene
446 expression cassette with primers ML3980/ML3981, that also carry 30 bp homology with the 3 end
447 of the corresponding genes. A specific single-guide RNA (sgRNA) was generated to introduce a
448 double-stranded break at the 3 of the *TgSUFC* gene, using primers ML3952/ML3953, and the
449 protospacer sequences were introduced in the Cas9-expressing pU6-Universal plasmid (Addgene, ref
450 #52694) (38). The TATi ΔKu80 cell line was transfected and transgenic parasites were selected with
451 chloramphenicol and cloned by serial limiting dilution.

452 **Generation of TgSUFC conditional knock-down and complemented cell lines.** The conditional
453 knock-down cell line for *TgSUFC* was generated based on the Tet-Off system using the
454 DHFR-TetO7Sag4 plasmid (74) using a CRISPR-based strategy. Using the DHFR-TetO7Sag4 plasmid as
455 a template, a PCR was performed with the KOD DNA polymerase (Novagen) to amplify the promoter
456 and the resistance gene expression cassette with primers ML4107/ML4108 that also carry 30 bp
457 homology with the 5 end of the *TgSUFC* gene. A specific single-guide RNA (sgRNA) was generated to
458 introduce a double-stranded break at the 5 of the *TgSUFC* locus. Primers used to generate the guide
459 were ML4109/ML4110 and the protospacer sequences were introduced in the pU6-Universal
460 plasmid (Addgene ref#52694) (38). The TgSUFC-HA cell line was transfected with the donor sequence
461 and the Cas9/guide RNA-expressing plasmid and transgenic parasites were selected with
462 pyrimethamine and cloned by serial limiting dilution.

463 The cKD TgSUFC-HA cell line was complemented by the addition of an extra copy of the *TgSUFC* gene
464 put under the dependence of a tubulin promoter at the *uracil phosphoribosyltransferase* (*UPRT*)
465 locus. *TgSUFC* (1,557 bp) whole cDNA sequence was amplified by reverse transcription (RT)-PCR with
466 primers ML4815/ML4816. They were then cloned downstream of the *tubulin* promoter sequence of
467 the pUPRT-TUB-Ty vector (25) to yield the pUPRT-TgSUFC plasmid. This plasmid was then linearized
468 prior to transfection of the mutant cell line. The recombination efficiency was increased by co-
469 transfecting with the Cas9-expressing pU6-UPRT plasmids generated by integrating *UPRT*-specific
470 protospacer sequences (with primers ML2087/ML2088 for the 3' and primers ML3445/ML3446 for
471 the 5') which were designed to allow a double-strand break at the *UPRT* locus. Transgenic parasites
472 were selected using 5-fluorodeoxyuridine and cloned by serial limiting dilution to yield the cKD
473 TgSUFC-HA comp cell line.

474

475 **Anti-TgPDH-E2 antibody production.** A polyclonal antibody was raised in rabbit against a peptide
476 (ISLIQAKGLSLISASSSPA) specific of TgPDH-E2 by the Proteogenix company. The peptide was
477 conjugated to Keyhole limpet haemocyanin carrier protein prior to immunization and the whole
478 serum was affinity-purified against the peptide for increased specificity.

479

480 **Immunoblot analysis.** Protein extracts from 10^7 freshly egressed tachyzoites were prepared in
481 Laemmli sample buffer, separated by SDS-PAGE and transferred onto nitrocellulose membrane using
482 the BioRad Mini-Transblot system according to the manufacturer's instructions. Rat monoclonal
483 antibody (clone 3F10, Roche) was used to detect HA-tagged proteins. Other primary antibodies used
484 were mouse monoclonal anti-TY tag (27), rabbit anti-lipoic acid antibody (ab58724, Abcam), mouse
485 anti-SAG1 (75), rabbit anti-CPN60 (76), mouse anti-actin (77), and rabbit anti-farnesyl polyclonal
486 antibody (PA1-12554, Life Technologies).

487

488 **Immunofluorescence microscopy.** For immunofluorescence assays (IFA), intracellular tachyzoites
489 grown on coverslips containing HFF monolayers, were either fixed for 20 min with 4% (w/v)
490 paraformaldehyde in PBS and permeabilized for 10 min with 0.3% Triton X-100 in PBS or fixed for
491 5 min in cold methanol (for SAG labelling). Slides/coverslips were subsequently blocked with 0.1%
492 (w/v) BSA in PBS. Primary antibodies used (at 1/1,000, unless specified) were rat anti-HA tag (clone
493 3F10, Roche), mouse anti-TY tag (27), rabbit anti-CPN60 (76), rabbit anti-IMC3 (78), mouse anti-SAG1
494 (75), and mouse anti-SAG3 (79). Staining of DNA was performed on fixed cells by incubating them for
495 5 min in a 1 µg/ml 4,6-diamidino-2-phenylindole (DAPI) solution. All images were acquired at the
496 Montpellier RIO imaging facility from a Zeiss AXIO Imager Z2 epifluorescence microscope driven by
497 the ZEN software v2.3 (Zeiss). Z-stack acquisition and maximal intensity projection was performed to
498 quantify apicoplast loss. Adjustments for brightness and contrast were applied uniformly on the
499 entire image.

500

501 **Electron Microscopy.** Parasites were pretreated for three days with ATc, and then used to infect HFF
502 monolayers and grown for an extra 24 hours in ATc. They were fixed with 2.5% glutaraldehyde in
503 cacodylate buffer 0.1 M pH7.4. Coverslips were then processed using a Pelco Biowave pro+ (Ted
504 Pella). Briefly, samples were postfixed in 1% OsO_4 and 2% uranyl acetate, dehydrated in acetonitrile
505 series and embedded in Epon 118 using the following parameters: Glutaraldehyde (150 W
506 ON/OFF/ON 1-min cycles); two buffer washes (40 s 150 W); OsO_4 (150 W ON/OFF/ON/OFF/ON 1-min
507 cycles); two water washes (40 s 150 W); uranyl acetate (100 W ON/OFF/ON 1-min cycles);
508 dehydration (40 s 150 W); resin infiltration (350 W 3-min cycles). Fixation and infiltration steps were
509 performed under vacuum. Polymerization was performed at 60°C for 48 hr. Ultrathin sections at
510 70 nM were cut with a Leica UC7 ultramicrotome, counterstained with uranyl acetate and lead
511 citrate and observed in a Jeol 1200 EXII transmission electron microscope from the MEA Montpellier
512 Electron Microscopy Platform. All chemicals were from Electron Microscopy Sciences, and solvents
513 were from Sigma.

514

515 **Plaque assay.** Confluent monolayers of HFFs were infected with freshly egressed parasites, which
516 were left to grow for 7 days in the absence or presence of ATc (unless stated). For some
517 experiments, the medium was supplemented with 50 µM palmitic acid (P0500, Sigma-Aldrich), 50
518 µM myristic acid (70082, Sigma-Aldrich), or 20 µM geranylgeranyol (G3278, Sigma-Aldrich). They
519 were then fixed with 4% v/v paraformaldehyde (PFA) and plaques were revealed by staining with a
520 0.1% crystal violet solution (V5265, Sigma-Aldrich).

521

522 **Gliding assay.** 10^7 freshly egressed parasites were resuspended in 300 µl of motility buffer (Ringer's
523 solution: 155 mM NaCl, 3 mM KCl, 2 mM $CaCl_2$, 1 mM $MgCl_2$, 3 mM NaH_2PO_4, 10 mM HEPES, 10 mM
524 glucose). 100 µl were deposited on poly-L-lysine coated microscope slides (J2800AMNZ, Thermo
525 Scientific), in a well delineated with a hydrophobic pen (PAP Pen, Kisker Biotech). Parasites were left
526 to glide for 15 minutes in an incubator at 37°C, then the suspension was carefully removed and
527 parasites were fixed with 4% (w/v) paraformaldehyde in PBS. Immunostaining was performed with
528 an anti-SAG1 antibody (75) as described above, but without permeabilization. Trail deposition images
529 were acquired with a 63x objective on a Zeiss AXIO Imager Z2 epifluorescence microscope and
530 processed with ImageJ v. 1.53f51, using the NeuronJ plugin as described previously (35).

531

532 **Lipidomic analyses.** Parasite lipidomic analyses were conducted as previously described (43, 80).
533 Briefly, the parasites were grown for 72 h in +/- ATc conditions within a confluent monolayer of HFF
534 in flasks (175 cm^2). At each time point, parasites were harvested as intracellular tachyzoites (1×10^7
535 cell equivalents per replicate) after syringe filtration with 3-µm pore size membrane. These parasites
536 were metabolically quenched by rapid chilling in a dry ice-ethanol slurry bath and then centrifuged
537 down at 4°C. The parasite pellet was washed with ice-cold PBS thrice, before transferring the final
538 pellet to a microcentrifuge tube. Then total lipids were extracted in chloroform/methanol/water
539 (1:3:1, v/v/v) containing PC (C13:0/C13:0), 10 nmol and C21:0 (10 nmol) as internal standards for
540 extraction. Polar and apolar metabolites were separated by phase partitioning by adding chloroform
541 and water to give the ratio of chloroform/methanol/water as 2:1:0.8 (v/v/v). For lipid analysis, the
542 organic phase was dried under N_2 gas and dissolved in 1-butanol to obtain 1µl butanol/10^7 parasites.

543 *Total lipid analysis* – The extracted total lipid sample was then added with 1 nmol pentadecanoic acid
544 (C15:0) as internal standard as stated before using Trimethylsulfonium hydroxide for total FA
545 content. Resultant FA methyl esters (FAMEs) were analyzed by GC-MS as previously described (45).
546 All FAMEs were identified by comparison of retention time and mass spectra from GC-MS with
547 authentic chemical standards. The concentration of FAMEs was quantified after initial normalization
548 to different internal standards and finally to parasite number.

549 Stable isotope metabolic labeling experiment.

550 *Tracking host-derived FAs – (monitoring parasite scavenging capacities)*

551 The HFF cells were grown (1×10^8 cell equivalents per replicate) to confluency in the presence of
552 stable isotope U-^{13}C-glucose at a final concentration of 800 µM added to a glucose-free DMEM.
553 These ^{13}C-pre labelled HFF were then infected with *Tg*LIPIN-ikD parasites in the presence of normal-
554 glucose containing DMEM under +/-ATc (0.5 µg/ml). The host HFF and parasites were metabolically
555 quenched separately, and their lipid content was quantified by GC-MS as described above. ^{13}C
556 incorporation to each FA was calculated as the percent of the metabolite pool containing one or
557 more ^{13}C atoms after correction for natural abundance and the amount of ^{13}C-carbon source in the
558 culture medium. The degree of the incorporation of ^{13}C into FAs (%carbon incorporation) was
559 determined by the mass isotopomer distribution of each FAMEs. Mass isotopomer distribution was
560 obtained from the shift in isotopic mass dependent on the amount of ^{12}C carbons compared to the
561 integration of ^{13}C carbon atoms. The total abundance of ^{13}C-labelled FAs was obtained by calculating
562 the concentration of all isotopomers of ^{13}C-labelled FAMEs and finally normalizing to authentic
563 internal standards and parasite number. The total abundance of ^{13}C-labelled FAs was analyzed
564 initially for HFF to check labelling of the metabolites (described previously). Later, the same was
565 calculated for parasites to confirm direct uptake of ^{13}C-labelled fatty acids from the host.

566

567 *Data availability*

568 All data are contained within the manuscript. Material described is available upon request from the
569 corresponding author.

570

571 *Supporting information*

572 This article contains supporting information.

Acknowledgments

We are grateful to B. Striepen, L. Sheiner, D. Soldati-Favre, M.J. Gubbels, V. Carruthers, and J.F. Dubremetz for sharing antibodies, strains and plasmids. We wish to thank K. Semenovskaya for technical help with some constructs. We also thank the Montpellier Rio Imaging facility for providing access to their microscopes, as well as the electron microscopy imaging facility of the University of Montpellier.

Funding and additional information

AC was supported by a fellowship from the Fondation pour la Recherche Médicale (Equipe FRM EQ20170336725). SB and CYB acknowledge support from the Labex Parafrap (ANR-11-LABX-0024), the Agence Nationale de la Recherche (ANR-21-CE44-0010 to CYB and SB, and ANR-19-CE15-0023 to SB). The funders had no role in study design, data collection and analysis, decision to publish, or preparation of the manuscript.

Conflict of interest

The authors declare that they have no conflicts of interest with the contents of this article.

References

1. White, N. J., Pukrittayakamee, S., Hien, T. T., Faiz, M. A., Mokuolu, O. A., and Dondorp, A. M. (2014) Malaria. *Lancet*. **383**, 723–735
2. Sanchez, S. G., and Besteiro, S. (2021) The pathogenicity and virulence of Toxoplasma gondii. *Virulence*. **12**, 3095–3114
3. Janouskovec, J., Horak, A., Obornik, M., Lukes, J., and Keeling, P. J. (2010) A common red algal origin of the apicomplexan, dinoflagellate, and heterokont plastids. *Proceedings of the National Academy of Sciences*. **107**, 10949–10954
4. van Dooren, G. G., and Striepen, B. (2013) The algal past and parasite present of the apicoplast. *Annu. Rev. Microbiol.* **67**, 271–289
5. van Dooren, G. G., and Hapuarachchi, S. V. (2017) The dark side of the chloroplast: biogenesis, metabolism and membrane biology of the apicoplast. in *Advances in Botanical Research*, pp. 145–185, Elsevier, **84**, 145–185
6. Seeber, F., and Soldati-Favre, D. (2010) Metabolic pathways in the apicoplast of apicomplexa. in *International Review of Cell and Molecular Biology*, pp. 161–228, **281**, 161–228
7. Biddau, M., and Sheiner, L. (2019) Targeting the apicoplast in malaria. *Biochem Soc Trans*. **47**, 973–983
8. Imlay, J. A. (2006) Iron-sulphur clusters and the problem with oxygen. *Mol Microbiol*. **59**, 1073–1082
9. Lill, R. (2009) Function and biogenesis of iron–sulphur proteins. *Nature*. **460**, 831–838

613 10. Braymer, J. J., Freibert, S. A., Rakwalska-Bange, M., and Lill, R. (2021) Mechanistic concepts of
614 iron-sulfur protein biogenesis in Biology. *Biochimica et Biophysica Acta (BBA) - Molecular Cell*
615 *Research*. **1868**, 118863
616 11. Aw, Y. T. V., Seidi, A., Hayward, J. A., Lee, J., Victor Makota, F., Rug, M., and van Dooren, G. G.
617 (2020) A key cytosolic iron-sulfur cluster synthesis protein localises to the mitochondrion of
618 Toxoplasma gondii. *Mol Microbiol*. 10.1111/mmi.14651
619 12. Pamukcu, S., Cerutti, A., Bordat, Y., Hem, S., Rofidal, V., and Besteiro, S. (2021) Differential
620 contribution of two organelles of endosymbiotic origin to iron-sulfur cluster synthesis and
621 overall fitness in Toxoplasma. *PLoS Pathog*. **17**, e1010096
622 13. Gisselberg, J. E., Dellibovi-Ragheb, T. A., Matthews, K. A., Bosch, G., and Prigge, S. T. (2013) The
623 Suf iron-sulfur cluster synthesis pathway is required for apicoplast maintenance in malaria
624 parasites. *PLoS Pathog.* **9**, e1003655
625 14. Haussig, J. M., Matuschewski, K., and Kooij, T. W. A. (2014) Identification of vital and
626 dispensable sulfur utilization factors in the Plasmodium apicoplast. *PLoS ONE*. **9**, e89718
627 15. Kumar, B., Chaubey, S., Shah, P., Tanveer, A., Charan, M., Siddiqi, M. I., and Habib, S. (2011)
628 Interaction between sulphur mobilisation proteins SufB and SufC: Evidence for an iron–sulphur
629 cluster biogenesis pathway in the apicoplast of Plasmodium falciparum. *International Journal*
630 *for Parasitology*. **41**, 991–999
631 16. Charan, M., Singh, N., Kumar, B., Srivastava, K., Siddiqi, M. I., and Habib, S. (2014) Sulfur
632 mobilization for Fe-S cluster assembly by the essential SUF pathway in the Plasmodium
633 falciparum apicoplast and its Inhibition. *Antimicrob. Agents Chemother.* **58**, 3389–3398
634 17. Charan, M., Choudhary, H. H., Singh, N., Sadik, M., Siddiqi, M. I., Mishra, S., and Habib, S. (2017)
635 [Fe-S] cluster assembly in the apicoplast and its indispensability in mosquito stages of the
636 malaria parasite. *FEBS J*. **284**, 2629–2648
637 18. Takahashi, Y., and Tokumoto, U. (2002) A third bacterial system for the assembly of Iron-Sulfur
638 clusters with homologs in archaea and plastids. *J. Biol. Chem.* **277**, 28380–28383
639 19. Hirabayashi, K., Yuda, E., Tanaka, N., Katayama, S., Iwasaki, K., Matsumoto, T., Kurisu, G.,
640 Outten, F. W., Fukuyama, K., Takahashi, Y., and Wada, K. (2015) Functional dynamics revealed
641 by the structure of the SufBCD complex, a novel ATP-binding cassette (ABC) protein that serves
642 as a scaffold for Iron-Sulfur cluster biogenesis. *Journal of Biological Chemistry*. **290**, 29717–
643 29731
644 20. Harb, O. S., and Roos, D. S. (2020) ToxoDB: functional genomics resource for Toxoplasma and
645 related organisms. *Methods Mol Biol*. **2071**, 27–47
646 21. Barylyuk, K., Koreny, L., Ke, H., Butterworth, S., Crook, O. M., Lassadi, I., Gupta, V., Tromer, E.,
647 Mourier, T., Stevens, T. J., Breckels, L. M., Pain, A., Lilley, K. S., and Waller, R. F. (2020) A
648 comprehensive subcellular atlas of the Toxoplasma proteome via hyperLOPIT provides spatial
649 context for protein functions. *Cell Host & Microbe*. 10.1016/j.chom.2020.09.011
650 22. Outten, F. W., Djaman, O., and Storz, G. (2004) A suf operon requirement for Fe-S cluster
651 assembly during iron starvation in Escherichia coli: suf operon role during iron starvation.
652 *Molecular Microbiology*. **52**, 861–872
653 23. Fox, B. A., Ristuccia, J. G., Gigley, J. P., and Bzik, D. J. (2009) Efficient gene replacements in
654 Toxoplasma gondii strains deficient for nonhomologous end joining. *Eukaryotic Cell*. **8**, 520–529
655 24. Huynh, M.-H., and Carruthers, V. B. (2009) Tagging of endogenous genes in a Toxoplasma
656 gondii strain lacking Ku80. *Eukaryot Cell*. **8**, 530–539
657 25. Sheiner, L., Demerly, J. L., Poulsen, N., Beatty, W. L., Lucas, O., Behnke, M. S., White, M. W., and
658 Striepen, B. (2011) A Systematic Screen to Discover and Analyze Apicoplast Proteins Identifies a
659 Conserved and Essential Protein Import Factor. *PLoS Pathog*. 10.1371/journal.ppat.1002392
660 26. Meissner, M., Brecht, S., Bujard, H., and Soldati, D. (2001) Modulation of myosin A expression
661 by a newly established tetracycline repressor-based inducible system in Toxoplasma gondii.
662 *Nucleic Acids Res.* **29**, E115

663 27. Bastin, P., Bagherzadeh, A., Matthews, K. R., and Gull, K. (1996) A novel epitope tag system to
664 study protein targeting and organelle biogenesis in Trypanosoma brucei. *Molecular and*
665 *Biochemical Parasitology*. **77**, 235–239
666 28. Francia, M. E., and Striepen, B. (2014) Cell division in apicomplexan parasites. *Nat. Rev.*
667 *Microbiol.* **12**, 125–136
668 29. Harding, C. R., and Meissner, M. (2014) The inner membrane complex through development of
669 Toxoplasma gondii and Plasmodium. *Cell Microbiol*. **16**, 632–641
670 30. Ouologuem, D. T., and Roos, D. S. (2014) Dynamics of the Toxoplasma gondii inner membrane
671 complex. *J Cell Sci*. **127**, 3320–3330
672 31. Gubbels, M.-J., Wieffer, M., and Striepen, B. (2004) Fluorescent protein tagging in Toxoplasma
673 gondii: identification of a novel inner membrane complex component conserved among
674 Apicomplexa. *Molecular and Biochemical Parasitology*. **137**, 99–110
675 32. Imlay, L., and Odom, A. R. (2014) Isoprenoid metabolism in apicomplexan parasites. *Curr Clin*
676 *Microbiol Rep*. **1**, 37–50
677 33. Thomsen-Zieger, N., Schachtner, J., and Seeber, F. (2003) Apicomplexan parasites contain a
678 single lipoic acid synthase located in the plastid. *FEBS Lett*. **547**, 80–86
679 34. Pierrel, F., Douki, T., Fontecave, M., and Atta, M. (2004) MiaB protein is a bifunctional radical-S-
680 adenosylmethionine enzyme involved in thiolation and methylation of tRNA. *J Biol Chem*. **279**,
681 47555–47563
682 35. Henkel, S., Frohnecke, N., Maus, D., McConville, M. J., Laue, M., Blume, M., and Seeber, F.
683 (2022) Toxoplasma gondii apicoplast-resident ferredoxin is an essential electron transfer
684 protein for the MEP isoprenoid-biosynthetic pathway. *J Biol Chem*. **298**, 101468
685 36. Frohnecke, N., Klein, S., and Seeber, F. (2015) Protein–protein interaction studies provide
686 evidence for electron transfer from ferredoxin to lipoic acid synthase in *Toxoplasma gondii*.
687 *FEBS Letters*. **589**, 31–36
688 37. Swift, R. P., Rajaram, K., Elahi, R., Liu, H. B., and Prigge, S. T. (2022) Roles of ferredoxin-
689 dependent proteins in the apicoplast of Plasmodium falciparum parasites. *mBio*.
690 10.1128/mbio.03023-21
691 38. Sidik, S. M., Huet, D., Ganesan, S. M., Huynh, M.-H., Wang, T., Nasamu, A. S., Thiru, P., Saeij, J.
692 P. J., Carruthers, V. B., Niles, J. C., and Lourido, S. (2016) A Genome-wide CRISPR Screen in
693 Toxoplasma Identifies Essential Apicomplexan Genes. *Cell*. **166**, 1423-1435.e12
694 39. Kennedy, K., Crisafulli, E. M., and Ralph, S. A. (2019) Delayed death by plastid inhibition in
695 apicomplexan parasites. *Trends in Parasitology*. **35**, 747–759
696 40. Jelenska, J., Crawford, M. J., Harb, O. S., Zuther, E., Haselkorn, R., Roos, D. S., and Gornicki, P.
697 (2001) Subcellular localization of acetyl-CoA carboxylase in the apicomplexan parasite
698 Toxoplasma gondii. *Proceedings of the National Academy of Sciences*. **98**, 2723–2728
699 41. Mazumdar, J., H Wilson, E., Masek, K., A Hunter, C., and Striepen, B. (2006) Apicoplast fatty acid
700 synthesis is essential for organelle biogenesis and parasite survival in Toxoplasma gondii. *Proc.*
701 *Natl. Acad. Sci. U.S.A.* **103**, 13192–13197
702 42. Ramakrishnan, S., Docampo, M. D., Macrae, J. I., Pujol, F. M., Brooks, C. F., van Dooren, G. G.,
703 Hiltunen, J. K., Kastaniotis, A. J., McConville, M. J., and Striepen, B. (2012) Apicoplast and
704 endoplasmic reticulum cooperate in fatty acid biosynthesis in apicomplexan parasite
705 Toxoplasma gondii. *J. Biol. Chem.* **287**, 4957–4971
706 43. Amiar, S., Katris, N. J., Berry, L., Dass, S., Duley, S., Arnold, C.-S., Shears, M. J., Brunet, C.,
707 Touquet, B., McFadden, G. I., Yamaryo-Botté, Y., and Botté, C. Y. (2020) Division and adaptation
708 to host environment of apicomplexan parasites depend on apicoplast lipid metabolic plasticity
709 and host organelle remodeling. *Cell Reports*. **30**, 3778-3792.e9
710 44. Liang, X., Cui, J., Yang, X., Xia, N., Li, Y., Zhao, J., Gupta, N., and Shen, B. (2020) Acquisition of
711 exogenous fatty acids renders apicoplast-based biosynthesis dispensable in tachyzoites of
712 Toxoplasma. *J Biol Chem*. **295**, 7743–7752

713 45. Dubois, D., Fernandes, S., Amiar, S., Dass, S., Katris, N. J., Botté, C. Y., and Yamaryo-Botté, Y.
714 (2018) Toxoplasma gondii acetyl-CoA synthetase is involved in fatty acid elongation (of long
715 fatty acid chains) during tachyzoite life stages. *J. Lipid Res.* **59**, 994–1004
716 46. Martins-Duarte, É. S., Carias, M., Vommaro, R., Surolia, N., and de Souza, W. (2016) Apicoplast
717 fatty acid synthesis is essential for pellicle formation at the end of cytokinesis in Toxoplasma
718 gondii. *J Cell Sci*. **129**, 3320–3331
719 47. Yeh, E., and DeRisi, J. L. (2011) Chemical rescue of malaria parasites lacking an apicoplast
720 defines organelle function in blood-stage Plasmodium falciparum. *PLoS Biol.* **9**, e1001138
721 48. Nair, S. C., Brooks, C. F., Goodman, C. D., Sturm, A., Strurm, A., McFadden, G. I., Sundriyal, S.,
722 Anglin, J. L., Song, Y., Moreno, S. N. J., and Striepen, B. (2011) Apicoplast isoprenoid precursor
723 synthesis and the molecular basis of fosmidomycin resistance in Toxoplasma gondii. *J. Exp.*
724 *Med*. **208**, 1547–1559
725 49. Li, Z.-H., Ramakrishnan, S., Striepen, B., and Moreno, S. N. J. (2013) Toxoplasma gondii relies on
726 both host and parasite isoprenoids and can be rendered sensitive to Atorvastatin. *PLoS Pathog*.
727 **9**, e1003665
728 50. Kennedy, K., Cobbold, S. A., Hanssen, E., Birnbaum, J., Spillman, N. J., McHugh, E., Brown, H.,
729 Tilley, L., Spielmann, T., McConville, M. J., and Ralph, S. A. (2019) Delayed death in the malaria
730 parasite Plasmodium falciparum is caused by disruption of prenylation-dependent intracellular
731 trafficking. *PLoS Biol*. **17**, e3000376
732 51. Li, Z.-H., King, T. P., Ayong, L., Asady, B., Cai, X., Rahman, T., Vella, S. A., Coppens, I., Patel, S.,
733 and Moreno, S. N. J. (2021) A plastid two-pore channel essential for inter-organelle
734 communication and growth of Toxoplasma gondii. *Nat Commun*. **12**, 5802
735 52. Suazo, K. F., Schaber, C., Palsuledesai, C. C., Odom John, A. R., and Distefano, M. D. (2016)
736 Global proteomic analysis of prenylated proteins in Plasmodium falciparum using an alkyne-
737 modified isoprenoid analogue. *Sci Rep*. **6**, 38615
738 53. Gisselberg, J. E., Zhang, L., Elias, J. E., and Yeh, E. (2017) The prenylated proteome of
739 Plasmodium falciparum reveals pathogen-specific prenylation activity and drug mechanism-of-
740 action. *Mol Cell Proteomics*. **16**, S54–S64
741 54. Jung, C., Lee, C. Y.-F., and Grigg, M. E. (2004) The SRS superfamily of Toxoplasma surface
742 proteins. *International Journal for Parasitology*. **34**, 285–296
743 55. Striepen, B., Yingxin He, C., Matrajt, M., Soldati, D., and Roos, D. S. (1998) Expression, selection,
744 and organellar targeting of the green fluorescent protein in Toxoplasma gondii. *Molecular and*
745 *Biochemical Parasitology*. **92**, 325–338
746 56. Fauquenoy, S., Morelle, W., Hovasse, A., Bednarczyk, A., Slomianny, C., Schaeffer, C., Van
747 Dorsselaer, A., and Tomavo, S. (2008) Proteomics and glycomics analyses of N-glycosylated
748 structures involved in Toxoplasma gondii-host cell interactions. *Molecular & Cellular*
749 *Proteomics*. **7**, 891–910
750 57. Luk, F. C. Y., Johnson, T. M., and Beckers, C. J. (2008) N-linked glycosylation of proteins in the
751 protozoan parasite Toxoplasma gondii. *Mol Biochem Parasitol*. **157**, 169–178
752 58. Vaughan, A. M., O'Neill, M. T., Tarun, A. S., Camargo, N., Phuong, T. M., Aly, A. S. I., Cowman, A.
753 F., and Kappe, S. H. I. (2009) Type II fatty acid synthesis is essential only for malaria parasite late
754 liver stage development. *Cellular Microbiology*. **11**, 506–520
755 59. Xu, X.-P., Elsheikha, H. M., Liu, W.-G., Zhang, Z.-W., Sun, L.-X., Liang, Q.-L., Song, M.-X., and Zhu,
756 X.-Q. (2021) The role of type II fatty acid synthesis enzymes FabZ, ODSCI, and ODSCII in the
757 pathogenesis of Toxoplasma gondii infection. *Front Microbiol*. **12**, 703059
758 60. Shunmugam, S., Arnold, C.-S., Dass, S., Katris, N. J., and Botté, C. Y. (2022) The flexibility of
759 Apicomplexa parasites in lipid metabolism. *PLoS Pathog*. **18**, e1010313
760 61. Krishnan, A., Kloehn, J., Lunghi, M., Chiappino-Pepe, A., Waldman, B. S., Nicolas, D., Varesio, E.,
761 Hehl, A., Lourido, S., Hatzimanikatis, V., and Soldati-Favre, D. (2020) Functional and
762 computational genomics reveal unprecedented flexibility in stage-specific Toxoplasma
763 metabolism. *Cell Host & Microbe*. 10.1016/j.chom.2020.01.002

764 62. Amberg-Johnson, K., and Yeh, E. (2019) Host cell metabolism contributes to delayed-death
765 kinetics of apicoplast inhibitors in Toxoplasma gondii. *Antimicrob Agents Chemother*. **63**,
766 e01646-18
767 63. Baggish, A. L., and Hill, D. R. (2002) Antiparasitic agent atovaquone. *Antimicrob Agents*
768 *Chemother*. **46**, 1163–1173
769 64. Huet, D., Rajendran, E., van Dooren, G. G., and Lourido, S. (2018) Identification of cryptic
770 subunits from an apicomplexan ATP synthase. *eLife*. **7**, e38097
771 65. Seidi, A., Muellner-Wong, L. S., Rajendran, E., Tjhin, E. T., Dagley, L. F., Aw, V. Y., Faou, P.,
772 Webb, A. I., Tonkin, C. J., and van Dooren, G. G. (2018) Elucidating the mitochondrial proteome
773 of Toxoplasma gondii reveals the presence of a divergent cytochrome c oxidase. *Elife*.
774 10.7554/eLife.38131
775 66. Hayward, J. A., Rajendran, E., Zwahlen, S. M., Faou, P., and van Dooren, G. G. (2021) Divergent
776 features of the coenzyme Q:cytochrome c oxidoreductase complex in Toxoplasma gondii
777 parasites. *PLoS Pathog*. **17**, e1009211
778 67. Maclean, A. E., Bridges, H. R., Silva, M. F., Ding, S., Ovciarikova, J., Hirst, J., and Sheiner, L.
779 (2021) Complexome profile of Toxoplasma gondii mitochondria identifies divergent subunits of
780 respiratory chain complexes including new subunits of cytochrome bc1 complex. *PLoS Pathog*.
781 **17**, e1009301
782 68. Agop-Nersesian, C., Naissant, B., Ben Rached, F., Rauch, M., Kretzschmar, A., Thiberge, S.,
783 Menard, R., Ferguson, D. J. P., Meissner, M., and Langsley, G. (2009) Rab11A-controlled
784 assembly of the inner membrane complex is required for completion of apicomplexan
785 cytokinesis. *PLoS Pathog*. **5**, e1000270
786 69. Venugopal, K., Chehade, S., Werkmeister, E., Barois, N., Periz, J., Lafont, F., Tardieux, I., Khalife,
787 J., Langsley, G., Meissner, M., and Marion, S. (2020) Rab11A regulates dense granule transport
788 and secretion during Toxoplasma gondii invasion of host cells and parasite replication. *PLoS*
789 *Pathog*. **16**, e1008106
790 70. Okada, M., Rajaram, K., Swift, R. P., Mixon, A., Maschek, J. A., Prigge, S. T., and Sigala, P. A.
791 (2021) *Critical role for isoprenoids in apicoplast biogenesis by malaria parasites*, Microbiology,
792 10.1101/2021.08.19.456988
793 71. Harding, C. R., Egarter, S., Gow, M., Jiménez-Ruiz, E., Ferguson, D. J. P., and Meissner, M. (2016)
794 Gliding associated proteins play essential roles during the formation of the inner membrane
795 complex of Toxoplasma gondii. *PLoS Pathog*. **12**, e1005403
796 72. Wichroski, M. J., and Ward, G. E. (2003) Biosynthesis of glycosylphosphatidylinositol Is essential
797 to the survival of the protozoan parasite Toxoplasma gondii. *Eukaryot Cell*. **2**, 1132–1136
798 73. Tomavo, S., Schwarz, R. T., and Dubremetz, J. F. (1989) Evidence for glycosyl-
799 phosphatidylinositol anchoring of Toxoplasma gondii major surface antigens. *Mol. Cell. Biol.* **9**,
800 4576–4580
801 74. Morlon-Guyot, J., Berry, L., Chen, C.-T., Gubbels, M.-J., Lebrun, M., and Daher, W. (2014) The
802 Toxoplasma gondii calcium-dependent protein kinase 7 is involved in early steps of parasite
803 division and is crucial for parasite survival. *Cell. Microbiol.* **16**, 95–114
804 75. Couvreur, G., Sadak, A., Fortier, B., and Dubremetz, J. F. (1988) Surface antigens of Toxoplasma
805 gondii. *Parasitology*. **97 (Pt 1)**, 1–10
806 76. Agrawal, S., van Dooren, G. G., Beatty, W. L., and Striepen, B. (2009) Genetic evidence that an
807 endosymbiont-derived endoplasmic reticulum-associated protein degradation (ERAD) system
808 functions in import of apicoplast proteins. *J. Biol. Chem.* **284**, 33683–33691
809 77. Herm-Gotz, A. (2002) Toxoplasma gondii myosin A and its light chain: a fast, single-headed,
810 plus-end-directed motor. *The EMBO Journal*. **21**, 2149–2158
811 78. Anderson-White, B. R., Ivey, F. D., Cheng, K., Szatanek, T., Lorestani, A., Beckers, C. J., Ferguson,
812 D. J. P., Sahoo, N., and Gubbels, M.-J. (2011) A family of intermediate filament-like proteins is
813 sequentially assembled into the cytoskeleton of Toxoplasma gondii. *Cell. Microbiol.* **13**, 18–31

79. Cesbron-Delauw, M. F., Tomavo, S., Beauchamps, P., Fourmaux, M. P., Camus, D., Capron, A., and Dubremetz, J. F. (1994) Similarities between the primary structures of two distinct major surface proteins of Toxoplasma gondii. *J Biol Chem*. **269**, 16217–16222
80. Dass, S., Shunmugam, S., Berry, L., Arnold, C.-S., Katris, N. J., Duley, S., Pierrel, F., Cesbron-Delauw, M.-F., Yamaryo-Botté, Y., and Botté, C. Y. (2021) Toxoplasma LIPIN is essential in channeling host lipid fluxes through membrane biogenesis and lipid storage. *Nat Commun*. **12**, 2813

Abbreviations

ABC (ATP-binding cassette), ATc (anhydrotetracycline), cKD (conditional knock-down), DMAPP (dimethylallyl diphosphate), ER (endoplasmic reticulum), ETC (electron transport chain), FA (fatty acid), FAME (fatty acid methyl ester), FASII (type II fatty acid synthase), FBS (fetal bovine serum), Fd (ferredoxin), Fe-S (iron-sulfur), GC-MS (gas chromatography-mass spectrometry), GGOH (geranylgeraniol), GPI (glycosylphosphatidylinositol), HA (hemagglutinin), HFF (human foreskin fibroblasts), IFA (immunofluorescence assay), IMC (inner membrane complex), IPP (isopentenyl diphosphate), ISC (iron–sulfur cluster), LipA (lipoic acid synthase A), LOPIT (localization of organelle proteins by isotope tagging), PDH (pyruvate dehydrogenase), surface antigen (SAG), SUF (sulfur utilization factor), TATi (tetracycline-inducible transactivator), UPRT (uracil phosphoribosyltransferase)

Figure legends

Figure 1. The *Toxoplasma gondii* functional homolog of SufC. A) Schematic representation of the molecular machinery for Fe-S cluster synthesis in the apicoplast of *T. gondii*. B) Alignment of the predicted amino acid sequence of TgSUFC and its homolog from *Escherischia coli*. Motifs that are potentially important for ATPase activity are outlined in blue. C) Functional complementation of bacterial mutants for SufC. Growth of 'wild-type' (WT) *E. coli* K12 parental strain, the SufC mutant strain and the mutant strain complemented ('comp') by the *T. gondii* homolog, was assessed by monitoring the optical density at 600 nm in the presence or not of an iron chelator (2,2'-bipyridyl, 'chel'). Values are mean from $n = 3$ independent experiments ±SEM. * denotes $p \leq 0.05$, Student's *t*-test, when comparing values obtained in the absence of chelator for the mutant cell line versus the complemented one.

Figure 2. Generation of conditional knock-down and complemented cell lines for the apicoplast-localized TgSUFC. A) Immunoblot analysis with anti-HA antibody shows precursor (p) and mature (m) forms of C-terminally HA-tagged TgSUFC and efficient down-regulation of the protein after 24 hours of incubation with ATc. Anti-SAG1 antibody was used as a loading control. B) HA-tagged TgSUFC (green) localizes to the apicoplast (labelled with marker TgCPN60, red) and is efficiently down-regulated upon addition of ATc for 24 hours. Scale bar represents 5 µm. DNA was labelled with DAPI.

856 Parasite shape is outlined. C) Immunoblot analysis of the conditional TgSUFC knock-down cell line
857 expressing a TY-tagged version of the protein shows similar processing profile and stable expression
858 after 48 hours of ATc addition. D) Immunofluorescence assay confirms co-localization of the
859 regulatable HA-tagged TgSUFC (green) and the TY-tagged additional copy (red), whose expression is
860 retained after 24 hours of incubation with ATc. Scale bar represents 5 µm. DNA was labelled with
861 DAPI. Parasite shape is outlined.

862

863 **Figure 3. Depletion of TgSUFC affects in vitro growth of the tachyzoites irresversibly.** A) Plaque
864 assays were carried out by infecting HFF monolayers with the TgSUFC2-HA conditional knock-down
865 and complemented cell lines. They were grown for 7 days ± ATc. B) Measurements of lysis plaque
866 areas highlight a significant defect in the lytic cycle when TgSUFC is depleted. Values are means of n =
867 3 experiments ± SEM. Mean value of a TATi ΔKu80 control grown in the presence of Atc (not shown
868 on the left) was set to 100% as a reference. **** denotes $p \leq 0.0001$, Student's t-test. Scale bar =
869 2mm. C) Plaque assays for the TgSUFC mutant was performed as described in A), but ATc was
870 washed out after 7 days (7d+ATc 7d-ATc) or not (14d+ATc), and parasites were left to grow for an
871 extra 7 days. No plaque was observed upon Atc removal. Shown are images from one representative
872 out of three independent experiments. Scale bar = 1mm. D) TgSUFC mutant and complemented cell
873 lines, as well as their parental cell line and the TATi ΔKu80 control, were grown in HFF in the
874 presence or absence of ATc for 48 hours, and subsequently allowed to invade and grow in new HFF
875 cells for an extra 24 hours in the presence of ATc. Parasites per vacuole were then counted. Values
876 are means ± SEM from n = 3 independent experiments for which 200 vacuoles were counted for each
877 condition.

878

879 **Figure 4. Depletion of TgNFS2 or TgSUFC leads to membrane defects during cell division.** A) TgNFS2-
880 HA and TgSUFC-HA conditional knock-down parasites as well as a TATi ΔKu80 control were grown in
881 the presence of ATc for up to 2 days and were stained with an anti-TgIMC3 antibody (in red, to
882 outline parasites and internal buds - top). Scale bar represents 5 µm. DNA was labelled with DAPI
883 (blue). B) The percentage of vacuoles presenting asynchronous division described in B) has been
884 quantified and is represented as a means of n = 3 experiments ± SEM (bottom). ** denotes $p \leq 0.01$,
885 Student's t-test. C) Electron microscopy analysis of TgNFS2-HA and TgSUFC-HA conditional mutants
886 grown for 4 days in the presence of ATc shows default in plasma membrane separation during
887 parasite division, as displayed on insets representing magnifications of selected parts of the
888 respective left image. D) cKD TgSUFC-HA parasites that were grown in the presence of ATc for 5 days
889 were co-stained with anti-TgIMC3 to outline the inner membrane complex and anti-TgCPN60 (an
890 apicoplast marker), which highlighted abnormal membrane structures and organelle segregation
891 problems. Scale bar represents 5 µm. DNA was labelled with DAPI.

892

893 **Figure 5. TgSUFC depletion impacts apicoplast-hosted Fe-S pathways.** A) cKD TgSUFC-HA parasites
894 were kept in the presence of ATc for up to five days and the aspect of the apicoplast was evaluated
895 by microscopic observation using the specific CPN60 marker. After 3 days, parasites egressed and
896 were used to reinvade new host cells for subsequent timepoints. Scale bar represents 5 µm. DNA was
897 labelled with DAPI. DIC: differential interference contrast. B) Using the labelling described in A),
898 apicoplast loss in vacuoles was monitored after two to five days of incubation with ATc. Data are
899 mean values from n = 3 independent experiments ±SEM. ns, not significant; * $p \leq 0.05$, **** $p \leq$
900 0.0001, Student's t-test. C) A decrease in the lipoylation of the E2 subunit of pyruvate dehydrogenase

901 (TgPDH-E2), which depends on the apicoplast-hosted Fe-S-containing lipoyl synthase LipA, was
902 observed by immunoblot using an anti-lipoic acid antibody on cell extracts from cKD TgSUFC-HA
903 parasites kept with ATc for an increasing period of time. A polyclonal antibody raised against PDH-E2
904 was used as a control for global abundance of the protein and for apicoplast integrity. TgACT1 was
905 used as a loading control. D) Decrease of lipoylated TgPDH-E2 was quantified by band densitometry
906 and normalized with the internal loading control. Data represented are mean ±SEM of $n = 3$
907 independent experiments. ns, not significant, *≤ 0.05, ** $p \leq 0.01$, *** $p \leq 0.001$, **** $p \leq 0.0001$,
908 ANOVA comparison.

909

910 **Figure 6. Lipidomic analysis of the consequences of TgNFS2 and TgSUFC depletion.** Ratio of total
911 lipid content for conditional knock-down cell lines for TgNFS2 (A) and TgSUFC (B) in the presence or
912 in the absence of ATc. (C) Stable isotope labelling combined to GCMS analyses allows the
913 quantification of host FA flux towards the parasite. ^{13}C incorporation levels of C16:0 illustrates a
914 significant increase of host scavenged fatty acids for the TgSUFC mutant. Data are mean from n=4
915 independent experiments ±SEM, * $p \leq 0.05$ Student's *t*-test

916

917 **Figure 7. Exogenous supplementation with short chain fatty acids only partially restore fitness of**
918 **cKD TgNFS2 and cKD TgSUFC mutant parasites *in vitro*.** Plaque assays were performed as described
919 in Figure 3A, in the absence or presence of 50 µM of palmitic (C16:0; A, B) or myristic (C14:0; C, D)
920 acid. Plaque sizes were measured and area was expressed as a percentage of the value obtained
921 after 7 days of growth in the absence of ATc. are mean values from $n = 3$ independent experiments
922 ±SEM. * $p \leq 0.05$, ** $p \leq 0.01$, Student's *t*-test. Palmitic acid allow partial restoration of plaques with
923 the cKD TgNFS2 mutant and to a lesser extent with the cKD TgSUFC mutant after 7 days of growth;
924 myristic acid partially restored plaques but only for the cKD TgNFS2 mutant and after two weeks of
925 incubation.

926

927 **Figure 8. The depletion of TgNFS2 or TgSUFC leads to mislocalization of GPI-anchored surface**
928 **antigens and impacts gliding motility.** A) TgNFS2 and TgSUFC conditional mutants were grown for
929 three days in the presence or absence of ATc and allowed to invade host cells for another 24 hours in
930 the presence or absence of ATc. Parasites were then co-stained for inner membrane complex marker
931 IMC3 (red) together with GPI-anchored protein SAG1 or SAG3 (green). As shown on insets
932 representing selected parts of the images, the depletion of TgNFS2 or TgSUFC leads to the
933 accumulation of SAGs in the vacuolar space (white arrowhead) or concentration at the apex or base
934 of the parasite (red arrowhead). Scale bar represents 10 µm. DNA was labelled with DAPI. B)
935 Quantification of the abnormal distribution of SAG labellings in vacuoles containing more than two
936 parasites. Data are mean values from $n = 3$ independent experiments ±SEM. **** $p \leq 0.0001$,
937 Student's *t*-test. C) Representative views of a gliding assay showing lower abundance of SAG1 trails
938 upon TgNFS2 or TgSUFC depletion (inverted grayscale images). Scale bar represents 10 µm. D)
939 Quantification of the trail to parasite ratio on at least ten randomly selected fields. Data are mean
940 values from $n = 3$ independent experiments ±SEM. ns, not significant; * $p \leq 0.05$, ** $p \leq 0.01$,
941 Student's *t*-test. E) Individual measurements of SAG1 trail lengths. Horizontal lines represent mean
942 values from $n = 3$ independent experiments ±SEM. ns, not significant; **** $p \leq 0.0001$, Student's *t*-
943 test.

944

945 **Figure 9. Schematic representation of th main celllular pathways that depend on apicoplast Fe-S**
946 **proteins.** For selected apicoplast-located Fe-S proteins squared red numbers represent CRISPR
947 fitness score of the corresponding gene (genes that contribute to *in vitro* parasite fitness are
948 represented by negative scores; values below −2.5 highlight increasing likelihood of being essential).
949 Fd: ferredoxin; IspG/IspH: oxidoreductases catalysing the last two steps of IPP/DMAPP synthesis;
950 LipA: lipoyl synthase; PDH-E2: E2 subunit of the pyruvate dehydrogenase complex; CoA: coenzyme A;
951 IPP: isopentenyl diphosphate; DMAPP: dimethylallyl diphosphate; FASII: fatty acid synthesis type II;
952 GPP: Geranyl diphosphate; FPP: farnesyl diphosphate; GGPP: Geranylgeranyl diphosphate; GPI:
953 Glycosylphosphatidylinisotol; dol-P: dolichol phosphate.

954

955 *Supporting Information*

956 This article contains supporting information (Figures S1-S5, Table S1)

957

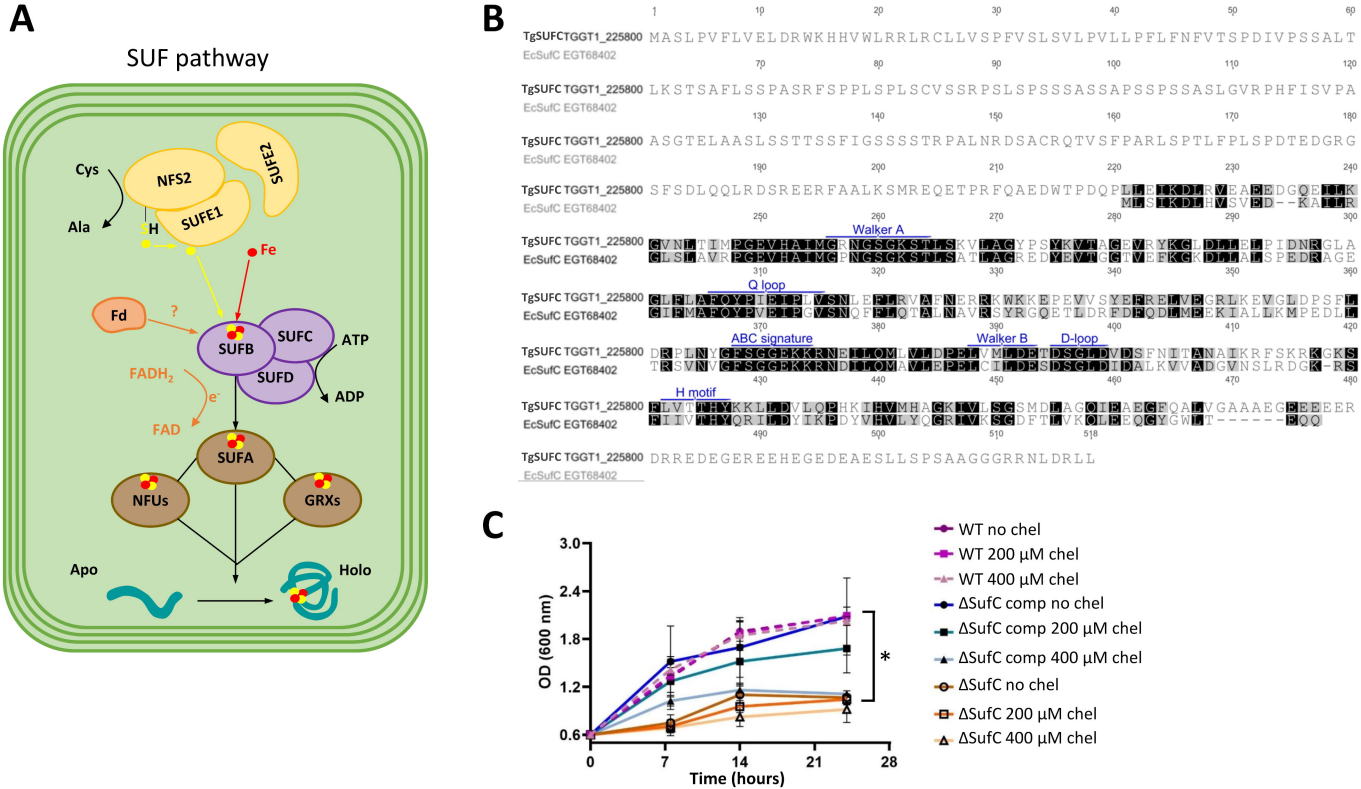
A
SUF pathway
Cys
Ala
NFS2
SUFE2
SUFE1
S
H
Fe
Fd
?
SUFB
SUFC
SUFD
ATP
ADP
FADH2
e-
FAD
SUFA
NFUs
GRXs
Apo
Holo
B
TgSUFC TGGT1_225800
EcSufC EGT68402
Walker A
Q loop
ABC signature
Walker B
D-loop
H motif
C
OD (600 nm)
Time (hours)
WT no chel
WT 200 µM chel
WT 400 µM chel
ΔSufC comp no chel
ΔSufC comp 200 µM chel
ΔSufC comp 400 µM chel
ΔSufC no chel
ΔSufC 200 µM chel
ΔSufC 400 µM chel
*

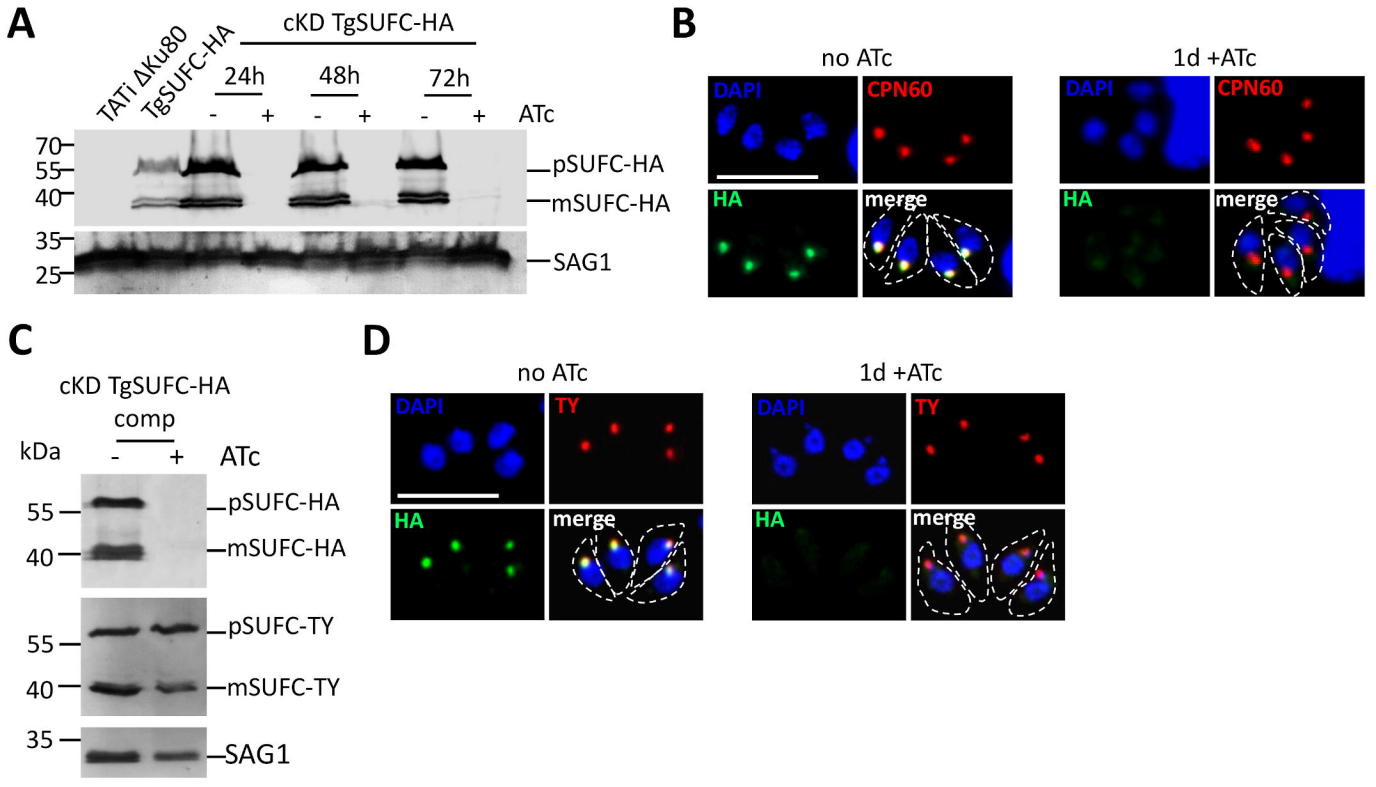
A
cKD TgSUFC-HA
TATi ΔKu80
TgSUFC-HA
24h
48h
72h
- + - + - +
ATc
70
55
40
35
25
pSUFC-HA
mSUFC-HA
SAG1
B
no ATc
1d +ATc
DAPI
CPN60
HA
merge
C
cKD TgSUFC-HA
comp
kDa
- +
ATc
55
40
pSUFC-HA
mSUFC-HA
55
40
pSUFC-TY
mSUFC-TY
35
SAG1
D
no ATc
1d +ATc
DAPI
TY
HA
merge

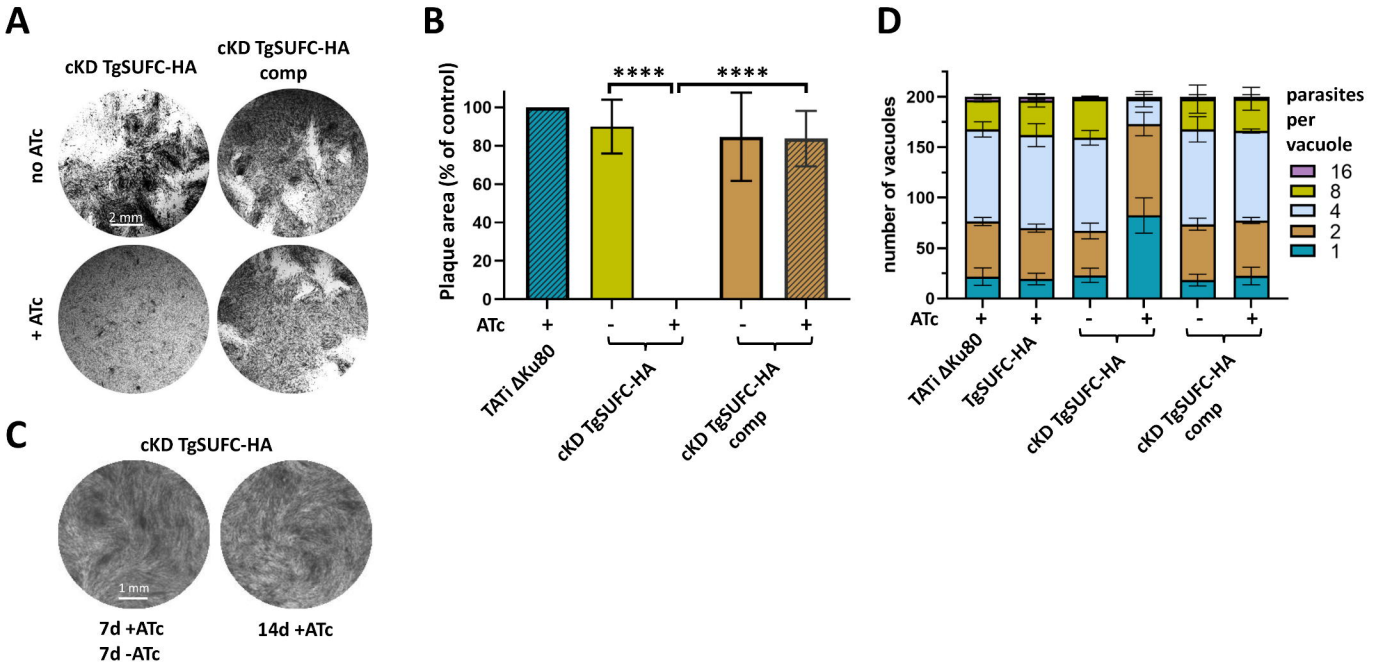
A
cKD TgSUFC-HA
cKD TgSUFC-HA comp
no ATc
+ ATc
2 mm
B
Plaque area (% of control)
****
****
ATc
TATi ΔKu80
cKD TgSUFC-HA
cKD TgSUFC-HA comp
C
cKD TgSUFC-HA
1 mm
7d +ATc
7d -ATc
14d +ATc
D
number of vacuoles
parasites per vacuole
16
8
4
2
1
ATc
TATi ΔKu80
TgSUFC-HA
cKD TgSUFC-HA
cKD TgSUFC-HA comp

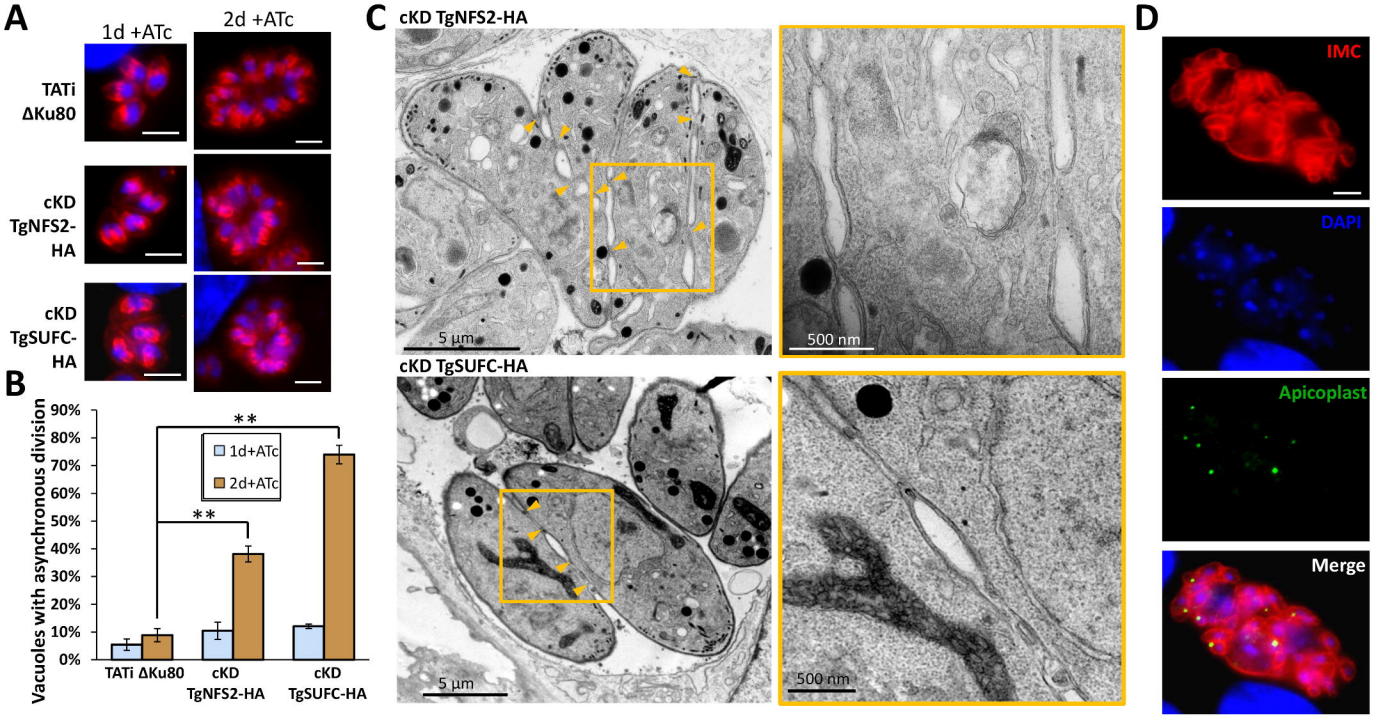
A
1d +ATc
2d +ATc
TATi ΔKu80
cKD TgNFS2-HA
cKD TgSUFC-HA
B
Vacuoles with asynchronous division
90%
80%
70%
60%
50%
40%
30%
20%
10%
0%
1d+ATc
2d+ATc
**
**
TATi ΔKu80
cKD TgNFS2-HA
cKD TgSUFC-HA
C
cKD TgNFS2-HA
5 µm
500 nm
cKD TgSUFC-HA
5 µm
500 nm
D
IMC
DAPI
Apicoplast
Merge

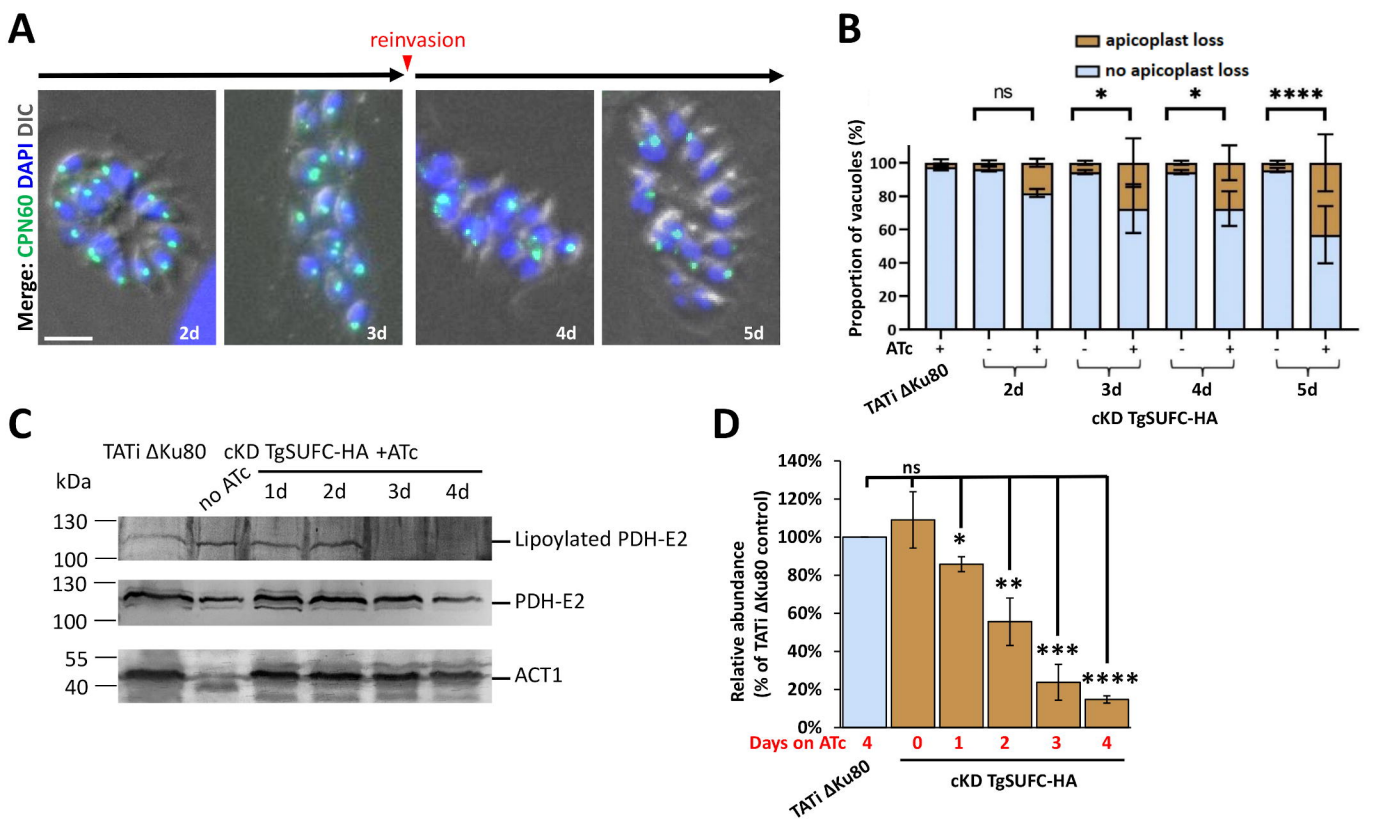
A
reinvasion
Merge: CPN60 DAPI DIC
2d
3d
4d
5d
B
apicoplast loss
no apicoplast loss
ns
*
*
****
Proportion of vacuoles (%)
100
80
60
40
20
0
ATc
+
-
+
-
+
-
+
-
+
TATi ΔKu80
2d
3d
4d
5d
cKD TgSUFC-HA
C
TATi ΔKu80
cKD TgSUFC-HA +ATc
kDa
no ATc
1d
2d
3d
4d
130
100
Lipoylated PDH-E2
130
100
PDH-E2
55
40
ACT1
D
140%
120%
100%
80%
60%
40%
20%
0%
Relative abundance
(% of TATi ΔKu80 control)
ns
*
**
***
****
Days on ATc
4
0
1
2
3
4
TATi ΔKu80
cKD TgSUFC-HA

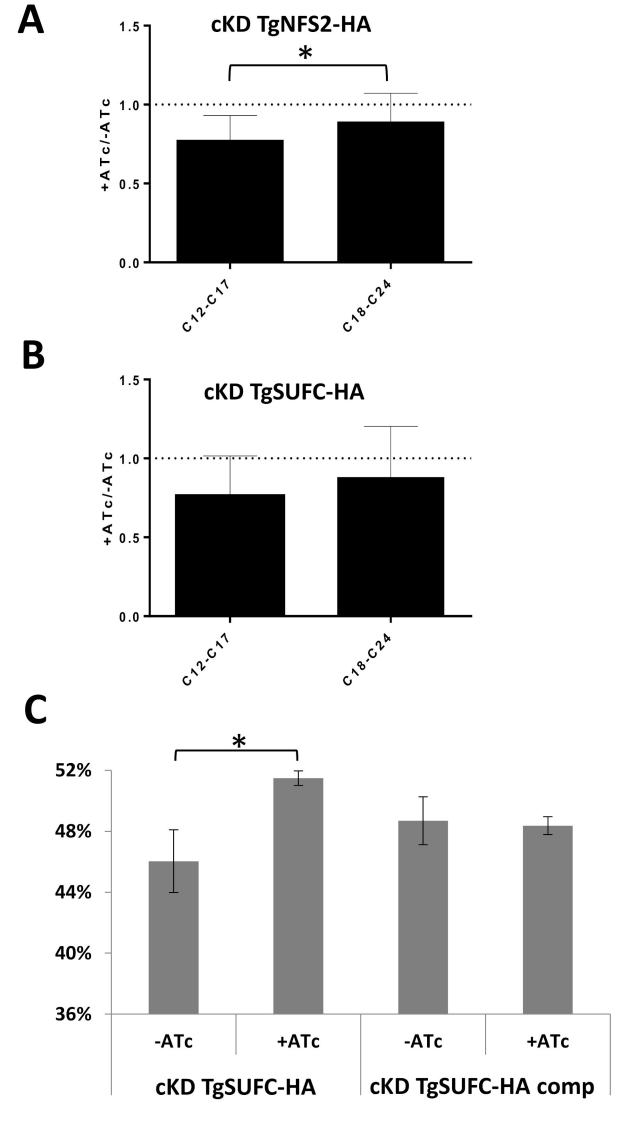
A
cKD TgNFS2-HA
*
+ATc/-ATc
1.5
1.0
0.5
0.0
C12-C17
C18-C24
B
cKD TgSUFC-HA
+ATc/-ATc
1.5
1.0
0.5
0.0
C12-C17
C18-C24
C
*
52%
48%
44%
40%
36%
-ATc
+ATc
-ATc
+ATc
cKD TgSUFC-HA
cKD TgSUFC-HA comp

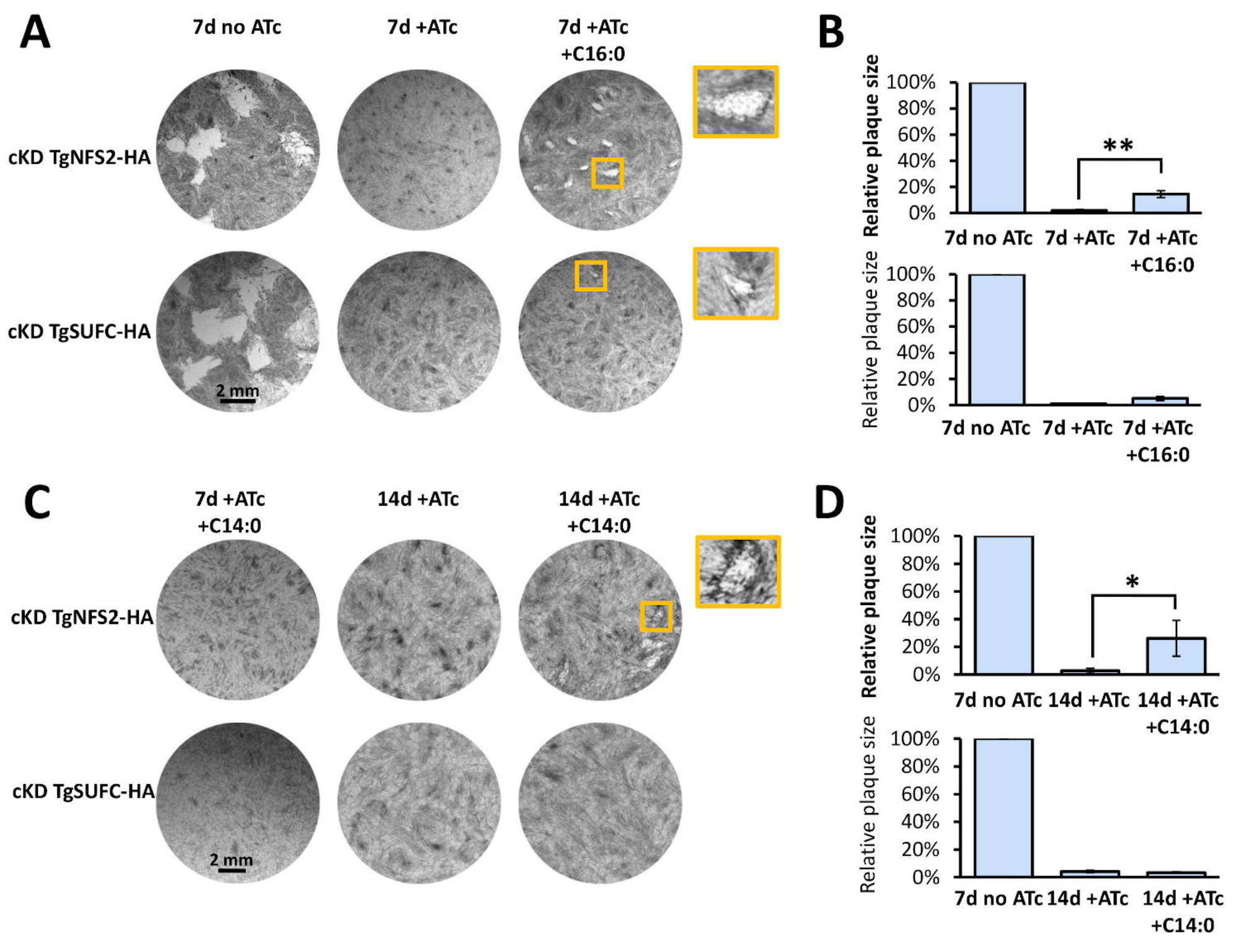
A
7d no ATc
7d +ATc
7d +ATc +C16:0
cKD TgNFS2-HA
cKD TgSUFC-HA
2 mm
B
Relative plaque size
100%
80%
60%
40%
20%
0%
**
7d no ATc
7d +ATc
7d +ATc +C16:0
C
7d +ATc +C14:0
14d +ATc
14d +ATc +C14:0
cKD TgNFS2-HA
cKD TgSUFC-HA
2 mm
D
*
7d no ATc
14d +ATc
14d +ATc +C14:0

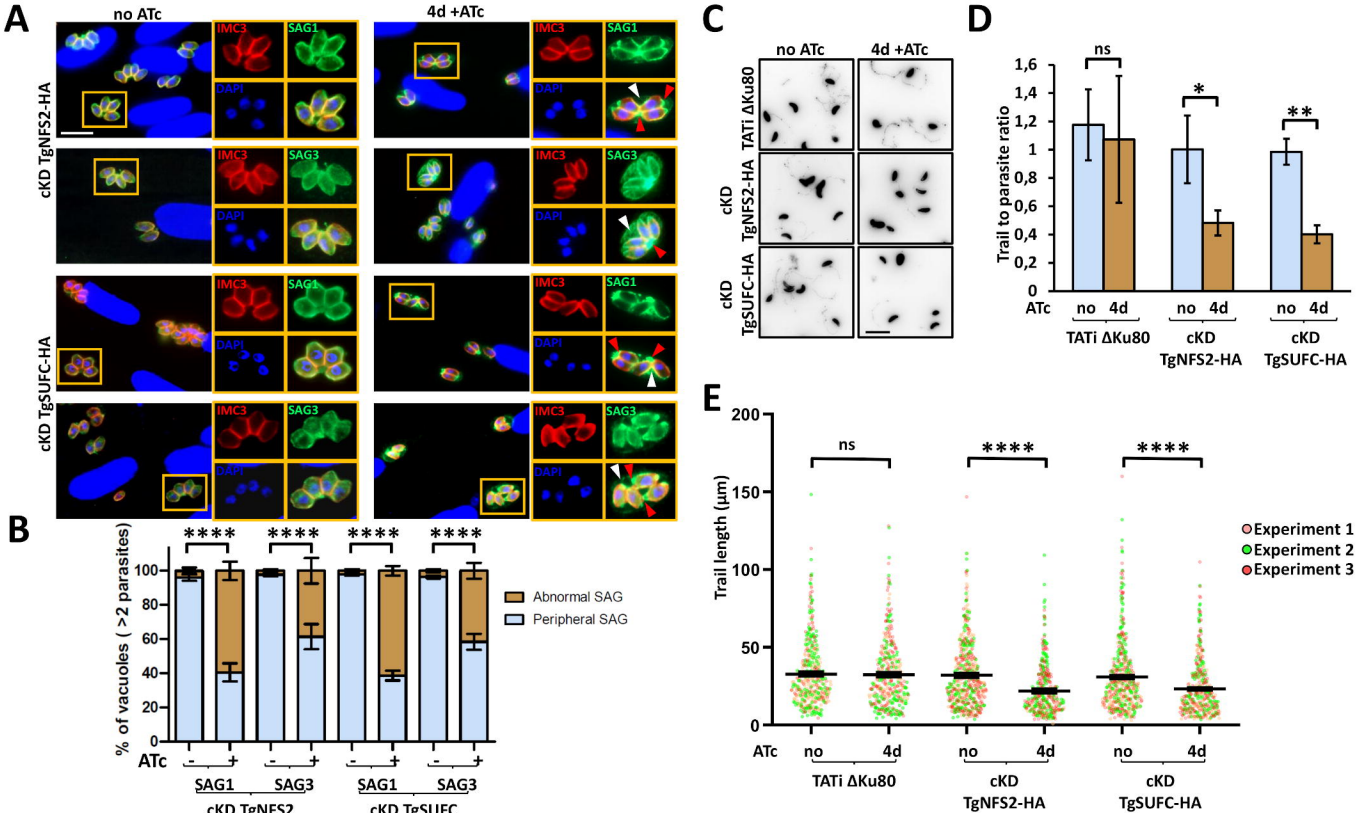
A
no ATc
4d +ATc
cKD TgNFS2-HA
cKD TgSUFC-HA
IMC3
SAG1
SAG3
DAPI
B
% of vacuoles (>2 parasites)
Abnormal SAG
Peripheral SAG
****
ATc
SAG1
SAG3
cKD TgNFS2
cKD TgSUFC
C
no ATc
4d +ATc
TATi ΔKu80
cKD TgNFS2-HA
cKD TgSUFC-HA
D
Trail to parasite ratio
ns
*
**
ATc
no
4d
TATi ΔKu80
cKD TgNFS2-HA
cKD TgSUFC-HA
E
Trail length (µm)
ns
****
Experiment 1
Experiment 2
Experiment 3

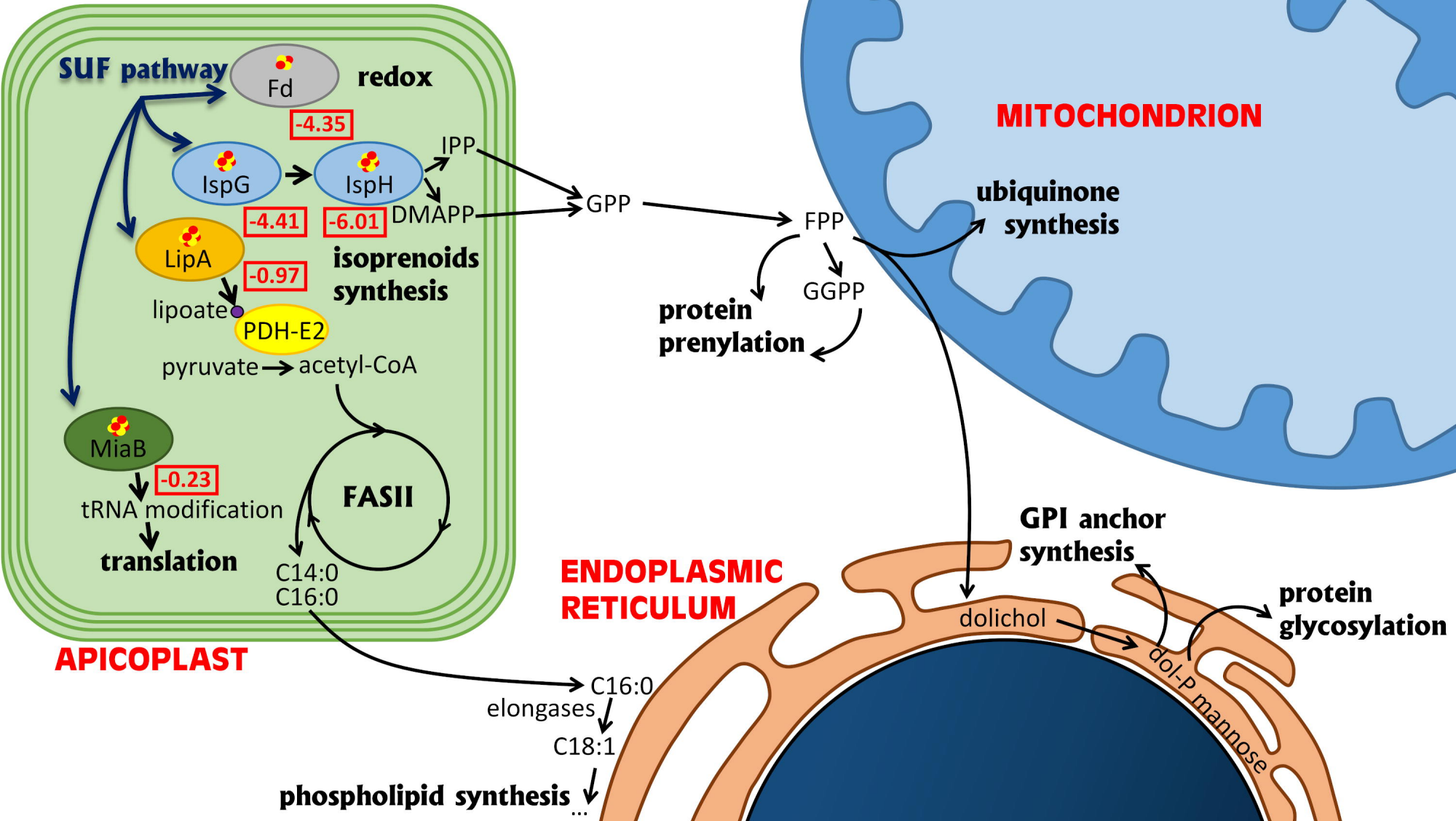
SUF pathway
Fd
redox
-4.35
IspG
IspH
IPP
DMAPP
-4.41
-6.01
LipA
-0.97
isoprenoids synthesis
lipoate
PDH-E2
pyruvate
acetyl-CoA
MiaB
-0.23
tRNA modification
translation
FASII
C14:0
C16:0
APICOPLAST
GPP
FPP
GGPP
protein prenylation
MITOCHONDRION
ubiquinone synthesis
GPI anchor synthesis
protein glycosylation
ENDOPLASMIC RETICULUM
dolichol
dol-P mannose
C16:0
elongases
C18:1
phospholipid synthesis